Original Article

MOLECULAR METABOLISM

# Deletion of intestinal epithelial AMP-activated protein kinase alters distal colon permeability but not glucose homeostasis

**Séverine Olivier [1,7], Camille Pochard [2,7], Hanna Diounou [1], Vanessa Castillo [3], Jordane Divoux [4], Joshua Alcantara [3], Jocelyne Leclerc [1], Sandra Guilmeau [1], Camille Huet [1], Wafa Charifi [1], Thibault V. Varin [5], Noëmie Daniel [5], Marc Foretz [1], Michel Neunlist [2], Benoit L. Salomon [4], Pradipta Ghosh [3,6], André Marette [5], Malvyne Rolli-Derkinderen [2,**], Benoit Viollet [1,*]**

## ABSTRACT

**Objective:** The intestinal epithelial barrier (IEB) restricts the passage of microbes and potentially harmful substances from the lumen through the paracellular space, and rupture of its integrity is associated with a variety of gastrointestinal disorders and extra-digestive diseases. Increased IEB permeability has been linked to disruption of metabolic homeostasis leading to obesity and type 2 diabetes. Interestingly, recent studies have uncovered compelling evidence that the AMP-activated protein kinase (AMPK) signaling pathway plays an important role in maintaining epithelial cell barrier function. However, our understanding of the function of intestinal AMPK in regulating IEB and glucose homeostasis remains sparse.
**Methods:** We generated mice lacking the two α1 and α2 AMPK catalytic subunits specifically in intestinal epithelial cells (IEC AMPK KO) and determined the physiological consequences of intestinal-specific deletion of AMPK in response to high-fat diet (HFD)-induced obesity. We combined histological, functional, and integrative analyses to ascertain the effects of gut AMPK loss on intestinal permeability *in vivo* and *ex vivo* and on the development of obesity and metabolic dysfunction. We also determined the impact of intestinal AMPK deletion in an inducible mouse model (i-IEC AMPK KO) by measuring IEB function, glucose homeostasis, and the composition of gut microbiota via fecal 16S rRNA sequencing.
**Results:** While there were no differences in *in vivo* intestinal permeability in WT and IEC AMPK KO mice, *ex vivo* transcellular and paracellular permeability measured in Ussing chambers was significantly increased in the distal colon of IEC AMPK KO mice. This was associated with a reduction in pSer425 GlV phosphorylation, a marker of leaky gut barrier. However, the expression of tight junction proteins in intestinal epithelial cells and pro-inflammatory cytokines in the lamina propria were not different between genotypes. Although the HFD-fed AMPK KO mice displayed suppression of the stress polarity signaling pathway and a concomitant increase in colon permeability, loss of intestinal AMPK did not exacerbate body weight gain or adiposity. Deletion of AMPK was also not sufficient to alter glucose homeostasis or the acute glucose-lowering action of metformin in control diet (CD)- or HFD-fed mice. CD-fed i-IEC AMPK KO mice also presented higher permeability in the distal colon under homeostatic conditions but, surprisingly, this was not detected upon HFD feeding. Alteration in epithelial barrier function in the i-IEC AMPK KO mice was associated with a shift in the gut microbiota composition with higher levels of *Clostridiales* and *Desulfovibrionales*.
**Conclusions:** Altogether, our results revealed a significant role of intestinal AMPK in maintaining IEB integrity in the distal colon but not in regulating glucose homeostasis. Our data also highlight the complex interaction between gut microbiota and host AMPK.


**Keywords** AMPK; Intestinal epithelial barrier (IEB); Permeability; Microbiota; Obesity; Metformin

## 1. INTRODUCTION

The intestinal epithelial barrier (IEB) is a single-cell layer that constitutes the largest and most important barrier to maintain an effective defense against intraluminal toxins, antigens, and enteric flora. Over the past decade, there has been increasing recognition of an association between disrupted IEB function and increased intestinal permeability or "leaky gut" in the pathogenesis and exacerbation of

[1]Université de Paris, Institut Cochin, INSERM, CNRS, F-75014 Paris, France [2]University of Nantes, INSERM, TENS, The Enteric Nervous System in Gut and Brain Diseases, IMAD, Nantes, France [3]Department of Cellular and Molecular Medicine, University of California San Diego, La Jolla, CA 92093, USA [4]Sorbonne Université, INSERM, CNRS, Centre d'Immunologie et des Maladies Infectieuses (CIMI), Paris, France [5]Québec Heart and Lung Research Institute (IUCPQ) & Institute for Nutrition and Functional Foods (INAF), Laval University Québec, Québec, Canada [6]Department of Medicine, University of California San Diego, La Jolla, CA 92093, USA

[7] Co-first authors.

*Corresponding author. Institut Cochin, 24 rue du Faubourg Saint Jacques 75014 Paris, France. Tel.: +33-(0)144412401. E-mail: benoit.viollet@inserm.fr (B. Viollet).

**Corresponding author. TENS, Faculté de Médecine, 1, Rue Gaston Veil, 44035 Nantes Cedex 1, France. Tel.: +33-(0)240412974. E-mail: malvyne.derkinderen@univ-nantes.fr (M. Rolli-Derkinderen).

Received October 28, 2020 • Revision received January 21, 2021 • Accepted February 1, 2021 • Available online 4 February 2021

https://doi.org/10.1016/j.molmet.2021.101183

 

many chronic diseases. Altered intestinal permeability contributes to diseases primarily occurring within the gastrointestinal system, such as inflammatory bowel disease (IBD) and celiac disease [1—3], and has been associated with clinical relapses in Crohn's disease [4]. Interestingly, the degree of intestinal permeability is also found to be associated with many risk factors for metabolic diseases [5,6], suggesting that a disrupted intestinal barrier could be an early event contributing to extra-digestive disease pathogenesis. The "leaky gut" concept has been extended to the development of obesity and its metabolic complications associated with systemic low-grade inflammation [7]. It has been proposed that the expansion of metabolic endotoxemia triggered by diet-induced obesity (DIO) in rodent models is a direct consequence of alterations of the gut barrier function and gut microbiota composition permitting the translocation of bacterial components such as lipopolysaccharides (LPS) into the systemic circulation and peripheral tissues [8—11]. Similar findings have been described in human obesity with increased circulating levels of LPS [12], a distinct gut microbiome signature [13] and impairment of intestinal barrier function [14] in various cohorts. Considering the contribution of increased intestinal permeability to digestive and systemic disease pathogenesis, alleviating gut leakiness appears to be an attractive therapeutic strategy.

AMPK is an evolutionarily conserved fuel-sensitive protein kinase and a cellular nutrient sensor implicated in regulating energy homeostasis [15]. Once activated by energy balance deficit, AMPK initiates metabolic changes to reprogram metabolism by inhibiting non-essential anabolic ATP-consuming processes while stimulating ATP-delivering catabolic pathways [15]. Recent evidence has expanded the paradigm of AMPK as a metabolic sensor and to the more global concept that AMPK has broad effects on cellular function [16]. Pioneering studies in renal MDCK cells described the important role of AMPK in maintaining epithelial cell barrier functions and demonstrated that pharmacological activation of AMPK protected the structure and barrier function of tight junctions [17,18]. The contribution of AMPK activation to intestinal barrier integrity has been recently illuminated in cultured intestinal epithelial cells under various stress conditions, including $Ca^{2+}$ depletion, ethanol-, LPS-, oxidative stress-, or dextran sulfate sodium (DSS)-induced intestinal barrier injury [19—26]. It has been reported that AMPK phosphorylates tight junction proteins and the associated proteins cingulin and GIV/Girdin [27—30], providing a possible regulatory mechanism of AMPK on intestinal barrier function. The gut microbiota is known to influence host health and play a key role in the development of obesity by acting through complex interactions [31—33]. Restoring intestinal health using microbiome-related strategies to attenuate inflammation and strengthen the epithelial barrier function has shown promising results in obese patients and DIO rodent models [7,34—38]. Interestingly, disruption of the gut microbiota has been associated with activation of AMPK in germ-free mice as reported in skeletal muscle and liver as well as in colonocytes to influence energy balance homeostasis [39,40]. Furthermore, fermentation products, such as short-chain fatty acids (SCFAs) synthesized directly by the commensal bacteria, can exert some of their actions in skeletal muscle, liver, and intestine by activating AMPK, thus contributing to improving whole-body metabolism by affecting lipid oxidation, insulin sensitivity [41,42], and intestinal barrier function [43—45]. Studies have also involved AMPK in the therapeutic potential of various pharmacological and nutritional compounds against DSS-induced colitis [46—49]. However, AMPK activation has been paradoxically linked to intestinal barrier dysfunction in chronic intestinal inflammatory conditions by decreasing ZO-1 expression [50]. Thus, there is evidence to suggest that, depending on the context, engaging AMPK activation may exert either a positive or negative influence on IEB integrity.

While there is promise in targeting the IEB by modulating AMPK, a deeper understanding of its regulatory role in epithelial homeostasis must be reached. To better understand the control exerted by AMPK on IEB function, we studied IEB permeability, junctional protein expression, gut inflammation susceptibility, and gut microbiota composition in animals lacking the two AMPKα1 and AMPKα2 catalytic subunits in intestinal epithelial cells in response to high-fat diet (HFD)-induced obesity.

## 2. MATERIALS AND METHODS

### 2.1. Reagents and antibodies

FITC- and TRITC-conjugated dextran (4 kDa) was obtained from TdB Consultancy AB. Horse radish peroxidase (HRP), red carmine, and carboxymethylcellulose (CMC) were acquired from Sigma. Primary antibodies directed against total AMPKα (#2532), AMPKβ1 (#4178), AMPKβ2 (#4148), AMPKγ2 (#2536), AMPKα phosphorylated at Thr-172 (#2531), total acetyl-CoA carboxylase 1/2 (ACC1/2) (#3676), ACC phosphorylated at Ser-79 (#3661), and β-actin (#4967) were purchased from Cell Signaling Technology. AMPKγ1 antibodies (#ab32508) were obtained from Abcam. ZO-1 antibodies were acquired from Cell Signaling Technology (#13663) and Thermo Fisher Scientific (#33-9100, Thermo Fisher Scientific). Anti-AMPKα1 and anti-AMPKα2 antibodies were kindly donated by Grahame Hardie (University of Dundee, Dundee, UK). HRP-conjugated secondary antibodies, goat anti-mouse IgG (#401215), and goat anti-rabbit IgG (#401393) were purchased from Calbiochem (EMD Millipore).

### 2.2. Experimental animals

All of the animal procedures were carried out in accordance with the EU guidelines for the protection of vertebra animals used for scientific purposes (2010/63/EU) and approved by the Institutional Animal Care and Use Committee no. 034 from Université de Paris (protocol number CEEA34.BV.157.12 and APAFIS 14911-2017120813494332 v5). The mice were maintained under controlled environmental conditions (12-h light/dark cycle) with free access to water and a standard mouse diet. Constitutive (IEC AMPK KO) and inducible (i-IEC AMPK KO) deletion of AMPKα1 and AMPKα2 in intestinal epithelial cells was obtained by crossing AMPK$\alpha1^{fl/fl}$/$\alpha2^{fl/fl}$ mice [51] and mice harboring Cre recombinase or tamoxifen-inducible Cre recombinase (CreERT2) under the control of the villin promoter, respectively [52]. All of the mice were kept on a C57/BL6J background. Routine genotyping was carried out by PCR on tail DNA using primer pairs for *AMPKα1* (forward 5'-TAT TGC TGC CAT TAG GCT AC-3' and reverse 5'-GAC CTG ACA GAA TAG GAT ATG CCC AAC CTC-3') to yield amplification products of 586 bp for *AMPKα1*$^{+/+}$ alleles and 682 bp for *AMPKα1*$^{fl/fl}$ alleles and for *AMPKα2* (forward 5′-GCT TAG CAC GTT ACC CTG GAT-3′ and reverse 5′-GTC TTC ACT GAA ATA CAT AGC A-3′) to yield amplification products of 260 bp for *AMPKα2*$^{+/+}$ alleles and 310 bp for *AMPKα2*$^{fl/fl}$ alleles and villin-Cre/CreERT2 (forward 5′-CAA GCC TGG CTC GAC GGC C-3′ complementary to the villin promoter and reverse 5′-CGC GAA CAT CTT CAG GTT CT-3′ complementary to the Cre coding sequence) to yield an amplification product of 220 bp [51—53]. To induce AMPK deletion in intestinal epithelial cells, the i-IEC AMPK KO mice were treated either for 5 days by intraperitoneal (IP) injections of tamoxifen (1 mg/day) or by 5 days of dietary supplementation (400 mg/kg TAM citrate, AT155T70400, Ssniff, Germany) at weaning prior to the control diet

 

(CD) and HFD challenge, followed one month later by 3 consecutive IP tamoxifen injections (1 mg/day). Littermates were used for all of the experiments.

### 2.3. Diet studies

Male mice were fed a CD (E15745-047, Ssniff, Germany) containing 70 kJ% carbohydrate, 10 kJ% fat, and 20 kJ% protein or HFD (E15742-347, Ssniff, Germany) containing 21 kJ% carbohydrate, 60 kJ% fat (primarily lard), and 19 kJ% protein. Starting at 10 weeks of age, co-housed WT and IEC AMPK KO mice received either a CD or HFD for 10 weeks. At weaning, WT and i-IEC AMPK KO mice were stratified on the basis of their genotype and were assigned to separate cages to receive either CD or HFD for 16 weeks. To analyze whole-body composition, unanesthetized mice were scanned using an NMR Minispec + LF90II (Bruker Optics).

### 2.4. Measurement of intestinal permeability *in vivo* and *ex vivo*

To analyze *in vivo* transcellular and paracellular intestinal permeability, the mice were gavaged with a mixed solution of 4 kDa of TRITC-conjugated dextran (2 g/kg) and HRP (0.1 g/kg) in 0.5% carboxymethylcellulose. The whole gut transit time was determined using 0.6 g/kg carmine red in the gavage solution and measuring the time of the appearance in the feces. For permeability measurements, the mice were placed in individual cages and tail tip blood samples were collected at 4 h after gavage. Plasma was analyzed for the TRITC-dextran 4 kDa concentration using an automatic fluorescence microplate reader at 544 nm excitation and 580 nm emission wavelengths to determine the paracellular permeability. To determine the transepithelial permeability, plasma HRP activity was measured using an enzyme activity assay with 3,3′,5,5′-tetramethylbenzidine reagent (TMB, BD Bioscience).

*Ex vivo* paracellular permeability of intestinal segments (jejunum, ileum, proximal colon, and distal colon) was determined by mounting the tissues in Ussing chambers (Physiological Instruments) as previously described [54]. Each chamber contains 2 ml of Ham (HAM/F12; Invitrogen) nutrient mixture maintained at 37 °C and continuously gasified with 95% $O_2$ and 5% $CO_2$. After 30 min of equilibration, 200 μL of apical medium was replaced by 200 μL of a mixed solution containing 4 kDa FITC-conjugated dextran (20 mg/ml) and HRP (3.75 mg/ml). The fluorescence level of the basolateral aliquots (150 μL) was measured every 30 min over a period of 180 min using an automatic fluorescence microplate reader (Varioskan, Thermo Fisher Scientific) at 485 nm excitation and 520 nm emission wavelengths.

### 2.5. Tolerance tests

Plasma glucose was assessed at 0, 20, 40, 60, 80, and 100 min after oral glucose administration (2 g/kg) in mice fasted for 6 h. Metformin tolerance was tested with a single oral administration of metformin (250 mg/kg) or vehicle (water) and after a 30 min challenge with an oral glucose bolus of 1.5 g/kg of body weight. For insulin tolerance tests, mice deprived of food for 4 h received an intraperitoneal injection of insulin (0.5 units/kg body weight, Actrapid, Novo Nordisk) and blood glucose levels were determined 0, 15, 30, 45, 60, and 90 min after injection. Blood glucose was measured in tail tip blood samples using a glucometer (Roche Diagnostics). The area under the curve was calculated using the trapezoidal rule.

### 2.6. In vivo GLP-1 secretion

Mice were fasted overnight and gavaged with 10 mg/kg of sitagliptin (MSD) 45 min before gastric gavage with a bolus of 25% glucose in olive oil. Blood was sampled 15 min after glucose/olive oil dosing gavage by retro-orbital venipuncture with heparin-coated capillaries in tubes containing 1% DPP IV inhibitor (Merck) and protease inhibitors (Sigma–Aldrich). The active GLP-1 plasma concentration was measured by ELISA (K150JVC-1, Meso Scale Diagnostics).

### 2.7. Plasma measurements

Blood was collected into heparin or EDTA-containing tubes and centrifuged to separate the plasma. Plasma lipid parameters were measured on an automated Monarch device (Instrumentation Laboratory Co). Plasma lipid parameters were determined enzymatically with added enzymatic reagents (DiaSys) for total cholesterol and triglyceride levels and an automated Monarch device (Instrumentation Laboratory Co) for non-esterified fatty acids (NEFA), glycerol, and β-hydroxybutyrate levels. Analysis of circulating cytokines (IL-6, TNF-α, and IFN-γ) was performed using a Meso Scale Discovery U-Plex kit for mouse cytokine profiling according to the manufacturer's instructions.

### 2.8. Indirect calorimetry

Indirect calorimetric measurements of whole energy expenditure, $O_2$ consumption, $CO_2$ production, respiratory exchange ratio (RER, calculated as volume of $CO_2$ produced to volume of $O_2$ consumed ratio), food intake, drink intake, and locomotor activity (beam breaks) were performed using an indirect calorimeter system (TSE PhenoMaster/LabMaster System). Energy expenditure, $CO_2$ production, and $O_2$ consumption were expressed by whole lean tissue mass extracted from an EchoMRI analysis. The mice were adapted for 60 h to metabolic chambers, and parameters were measured for 5 consecutive days. Room temperature was kept constant (22 °C ± 1 °C). The mice were assessed under standard CD nutritional conditions and a HFD challenge for 10 weeks.

### 2.9. Fecal sample collection, DNA extraction, and 16s gene-based analysis

Fresh fecal samples were collected in sterile tubes, stored at −80 °C, and processed for DNA extraction using a ZymoBIOMICS DNA Microprep kit (Zymo Research). Extracted DNA (100 ng) was processed for 16S rRNA amplification of the V3–V4 region and fecal microbiota profiling as previously described [55]. Sequence reads were analyzed using the dada2 package (v1.5.0; [56]) in R (http://www.R-project.org). Forward and reverse reads were first trimmed to remove low-quality regions. Sequences with an expected error threshold >2 and > 4 for the forward and reverse reads, respectively, with ambiguous bases and quality scores less than or equal to 2 were discarded. Denoised forward and reverse reads were merged and searched for chimeras. Taxonomic assignment of amplicon sequence variants (ASVs) was performed using the RDP classifier algorithm (v2,2; [57]) trained against the Silva database 132 [58]. To avoid biases generated in the sequencing depth, ASV tables were rarified to an even depth of 19,991 sequences per sample. Potentially spurious ASVs with a total abundance lower than 0.05% and that appeared less than three times in the entire dataset were removed.

### 2.10. Fecal lipocalin-2 quantification

Quantification of fecal lipocalin-2 (Lcn-2) levels was performed as previously described [59]. Briefly, frozen fecal samples were homogenized in sterile PBS at 100 mg/ml and then centrifuged at 12,000 rpm for 10 min at 4 °C. Lcn-2 levels were measured in the supernatants using a Duoset Murine Lcn-2 ELISA kit (R&D Systems).

 

### 2.11. Intestinal epithelial cell fractionation and lamina propria cell isolation

To isolate intestinal epithelial cells, either "whole" (scraping the epithelial lining) or "villus enriched" cell isolation methods were used. Briefly, intestinal fragments were isolated, opened longitudinally, and rinsed with PBS. The tissues were rotated for 30 min at 4 °C in PBS containing 1.5 mM EDTA and a protease inhibitor cocktail (Complete Protease Inhibitor Cocktail; Roche). Cells were recovered by centrifugation at 1500 rpm at 4 °C for 5 min and cell pellets were snap frozen in liquid nitrogen and stored at −80 °C. For cell fractionation, the sequential isolation of intestinal epithelial cells along the crypt—villus axis was performed as previously described [60,61]. To isolate cells from the lamina propria, a Miltenyi Lamina Propria Dissociation kit for mice (Miltenyi) was used according to the manufacturer's instructions.

### 2.12. Quantitative real-time PCR analysis

Fragments of the different intestinal segments were lysed in RA1 buffer (Macherey—Nagel), and total RNA extraction was performed with a Nucleospin RNA II kit according to the manufacturer's instructions (Macherey—Nagel). One μg of purified mRNA was denatured and retro-transcribed using Superscript III reverse transcriptase (Invitrogen). PCR amplifications were performed using an Absolute Blue SYBR green fluorescein kit (Roche) and analyzed on a StepOnePlus system (Life Technologies). The relative gene expression was calculated using the comparative Ct ($2^{-\Delta\Delta Ct}$) method, in which values were normalized to a housekeeping gene (ribosomal protein S6). The following primers (Sigma—Aldrich) were used: tumor necrosis factor alpha (TNFα, #NM_013693.3, forward primer 5′-GAA CTT CGG GGT GAT CGG TCC-3′, and reverse primer 5′-GCC ACT CCA GCT GCT CCT CC-3′), interleukin 1 beta (IL-1β, #NM_008361.4, forward primer 5′-GCC TCG TGC TGT CGG ACC CAT A-3′, and reverse primer 5′-TTG AGG CCC AAG GCC ACA GGT-3′), interleukin 6 (IL-6, #NM_031168.2, forward primer 5′-TCC AGT TGC CTT CTT GGG AC-3′, and reverse primer 5′-AGT CTC CTC TCC GGA CTT GT-3′), zona occludens-1 (ZO-1, #NM_009386.2, forward primer 5′-AAG AAT ATG GTC TTC GAT TGG-3′, and reverse primer 5′-ATT TTC TGT CAC AGT ACC ATT TAT CTT C-3′), occludin (#NM_008756.2, forward primer 5′-GGT TAA AAA TGT GTC TGC AGG CAC-3′, and reverse primer 5′-GAG GCT GCC TGA AGT CAT CCA C-3′), zona occludens-2 (ZO-2, #NM_001198985.1, forward primer 5′-CTAGACCCCCAGAGCCCCAGAAA-3′, and reverse primer 5′-TCGCAGGAGTCCACGCATACAAG-3′), claudin 1 (#NM_016674.4, forward primer 5′-AATTTCAGGTCTGGCGACAT-3′, and reverse primer 5′-GGCCAAATTCATACCTGGCA-3′), claudin 2 (#NM_016675.4, forward primer 5′-GAAAGGACGGCTCCGTTTTC-3′, and reverse primer 5′-TCTTCGGAGCCTGTTTGCTT-3′), claudin 3 (#NM_009902.4, forward primer 5′-GCCCCAGGAGAGGAGCCGTTAA-3′, and reverse primer 5′-GCCGATGAAGGCCGAAACGC-3′), and ribosomal protein S6 (RPS6, #NM_001010.2, forward primer 5′-CCA AGC TTA TTC AGC GTC TTG TTA CTC C-3′, and reverse primer 5′-CCC TCG AGT CCT TCA TTC TCT TGG C-3′).

### 2.13. Western blotting

Cells were lysed in ice-cold lysis buffer (50 mM of Tris, pH 7.4, 1% Triton X-100, 150 mM of NaCl, 1 mM of EDTA, 1 mM of EGTA, 10% glycerol, 50 mM of NaF, 5 mM of sodium pyrophosphate, 1 mM of $Na_3VO_4$, 25 mM of sodium-β-glycerophosphate, 1 mM of DTT, and 0.5 mM of PMSF) and protease inhibitor cocktail (Complete Protease Inhibitor Cocktail, Roche) and sonicated on ice for 15 s to shear DNA and reduce viscosity. Intestine samples isolated from the duodenum, jejunum, ileum, and colon were homogenized in ice-cold lysis buffer using a ball-bearing homogenizer (Retsch). The homogenate was centrifuged for 10 min at 10,000×*g* at 4 °C, and the supernatants were removed to determine the total protein content with a BCA protein assay kit (Thermo Fisher Scientific). Proteins (25 μg) were separated by SDS-PAGE in precast 4-15% polyacrylamide gels (Bio-Rad) and the resulting bands were transferred to nitrocellulose membranes. Equal loading was checked by membrane staining with Ponceau Red before blocking with Tris-buffered saline supplemented with 0.2% NP40 and 5% non-fat dry milk for 30 min at room temperature. Immunoblotting was performed following standard procedures. Total pan-AMPKα, AMPKα1, α2, β1, β2, γ1, γ2, β-actin, phosphorylated AMPK, and ACC were probed from separated membranes. The signals were detected with chemiluminescence reagents (EMD Millipore) using ImageQuant LAS 4000 (GE Healthcare) or X-ray films. Band intensities were quantified using an ImageJ densitometry analysis and ratios of AMPKα1/AMPKα2 were calculated.

### 2.14. Flow cytometry analysis

Immunophenotyping of adipose tissue and colon biopsies was performed as follows. The mice were anesthetized using xylazine/ketamine and perfused by intra-cardiac injections of cold PBS before harvesting tissues. Small pieces of colon removed from Peyer patches, epithelium, and adipose tissues were digested in type IV collagenase (1 mg/ml) and DNase I (10 μg/ml) for 30 min at 37 °C, followed by Percoll gradient (40-80%) separation. Single-cell suspensions were then stained with live-dead e780 (Thermo Fisher Scientific) for 10 min in cold PBS followed by 20 min of incubation in cold PBS 3% FBS with the following mAbs: anti-$CD45_{LCA}$ (30-F11, BD Biosciences), anti-CD11b (M1/70, BD Biosciences), anti-CD11c (HL3 BD Biosciences), anti-IA/E (M5/114.15.2, BD Biosciences), anti-Ly6C (AL-21, BD Biosciences), anti-Ly6G (1A8, BD Biosciences), and anti-F4/80 (BM8, Thermo Fisher Scientific). Cells were acquired on a Fortessa X20 cytometer (BD Biosciences) and analyzed using FlowJo software (BD Biosciences). Myeloid cell populations were defined as follows: monocytes (CD45+ CD11b+ Ly-6C+), dendritic cells (CD45+ CD11c+ IA/E+), macrophages (CD45+ CD11b+ F4/80+), and neutrophils (CD45+ Ly-6C+ Ly-6G+).

### 2.15. Immunohistochemistry (pSer425 GIV)

Formalin-fixed paraffin-embedded colon sections 4 μm thick were cut and placed on glass slides coated with poly-L-lysine, followed by deparaffinization and hydration as previously described [28]. Heat-induced epitope retrieval was performed using sodium citrate buffer (pH 6) in a pressure cooker. Tissue sections were incubated with 0.3% hydrogen peroxidase for 15 min to block endogenous peroxidase activity, followed by incubation with primary antibodies for 30 min in a humidified chamber at room temperature. Antibodies used for immunostaining were anti-pS245 GIV (1:50, anti-rabbit antibody). Immunostaining was visualized with labeled streptavidin-biotin using 3,3′-diaminobenzidine as a chromogen and counterstained with hematoxylin. Immunohistochemistry (IHC) images were randomly sampled at different 150 × 100 pixel regions of interest (ROI). The ROIs were analyzed using IHC Profiler (https://doi.org/10.1371/journal.pone.0096801). IHC Profiler used a spectral deconvolution method of DAB/hematoxylin color spectra using optimized optical density vectors of the color deconvolution plugin to properly segregate the DAB color spectra. The histogram of the DAB intensity was divided into 4 zones: high positive (0—60), positive (61—120), low positive (121—180), and

 

negative (181–235). High positive, positive, and low positive percentages were combined to compute the final percentage positive for each ROI. The range of values for the percent positive was compared among the different experimental groups.

### 2.16. Transmission electron microscopy

Colon samples were fixed in 3% glutaraldehyde and 0.1 M sodium phosphate buffer (pH 7.4) for 24 h at 4 °C, post-fixed with 1% osmium tetroxide, dehydrated with 100% ethanol, and embedded in epoxy resin. For ultrastructure analysis, ultrathin slices (70-100 nm thick) were cut from the resin blocks with a Reichert Ultracut S ultramicrotome (Reichert Technologies, Depew, NY, USA), stained with lead citrate and uranyl acetate, and examined with a transmission electron microscope (model 1011; JEOL, Tokyo, Japan) at the Cochin Institute electron microscopy facility.

### 2.17. Statistical analyses

The R phyloseq package (v1.26.1) was used to perform all of the microbiota diversity analyses. The Shannon index was calculated to assess alpha diversity. Differences in beta diversity were visualized using a principal coordinate analysis (PCoA) based on the unweighted UniFrac distance calculated from the 16S rRNA gene sequencing data. Differentially abundant taxa between the groups were detected using the metagenomics biomarker discovery tool linear discriminant analysis effect size (LefSe) [62]. A logarithmic LDA score of $>2.5$ was used as a threshold.

Data are presented as means ± SEM. Results were analyzed using Student's t test and 2- or 3-way ANOVA with or without repeated measurements as appropriate followed by a Bonferroni post hoc test using GraphPad Prism software. Values of $p < 0.05$ were considered statistically significant.

## 3. RESULTS

### 3.1. AMPK α1 and α2 catalytic subunits were expressed along the GI tract

To study the physiological role of AMPK in mouse GI tract, we first examined the distribution of AMPK isoforms in intestinal epithelial cells (IECs) isolated from the proximal and distal segments of the duodenum, jejunum, ileum, and colon. We found that the AMPKα1 and AMPKα2 catalytic subunits and the AMPKβ1, AMPKβ2, AMPKγ1, and AMPKγ2 regulatory subunits were expressed at various levels along the small and large intestines (Figure 1A). Interestingly, an increasing gradient of both AMPKα1 and AMPKα2 protein expression was observed along the GI antero-posterior axis from the duodenum to the colon (Figure 1A). We also analyzed the patterns of AMPKα1 and AMPKα2 expression in the duodenum crypt–villus axis, where spatial expression changes and sub-specialization heterogeneity is well

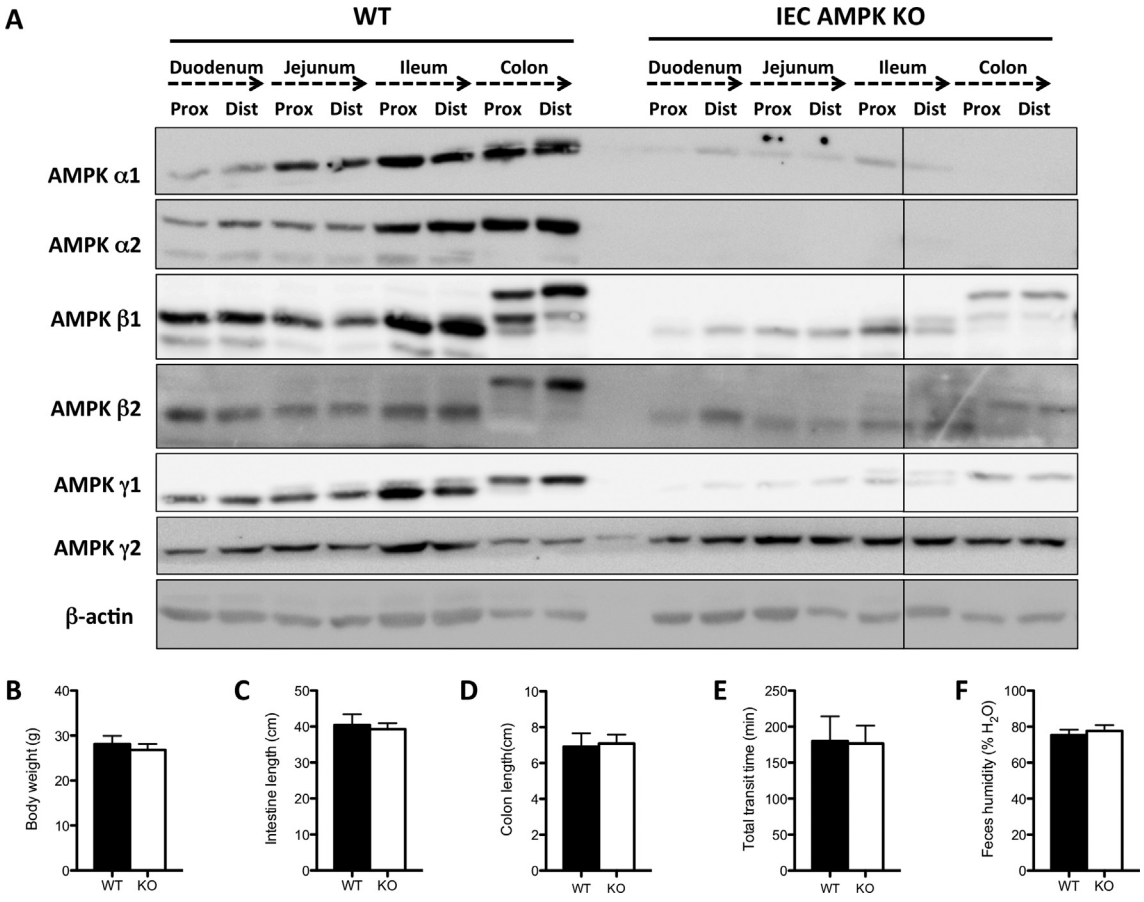


**Figure 1: AMPKα1 and AMPKα2 deletion in mouse GI tract**. (A) Western blotting analysis of AMPKα1, α2, β1, β2, γ1, and γ2 expression in intestinal epithelial cells (IECs) isolated from the duodenum, jejunum, ileum, and colon of WT and IEC AMPK KO mice. β-actin was used as a loading control. IEC-specific AMPK deletion was obtained by expressing Cre-recombinase driven by the villin promoter. Measurement of (B) body weight, (C) intestine length, (D) colon length, (E) total transit time, and (F) feces humidity in WT and IEC AMPK KO mice. n = 6–8 mice. All of the data are expressed as means ± SEM. Statistical analysis was performed using Student's t test. Black bars, WT mice (WT); white bars, IEC AMPK KO mice (KO).

 

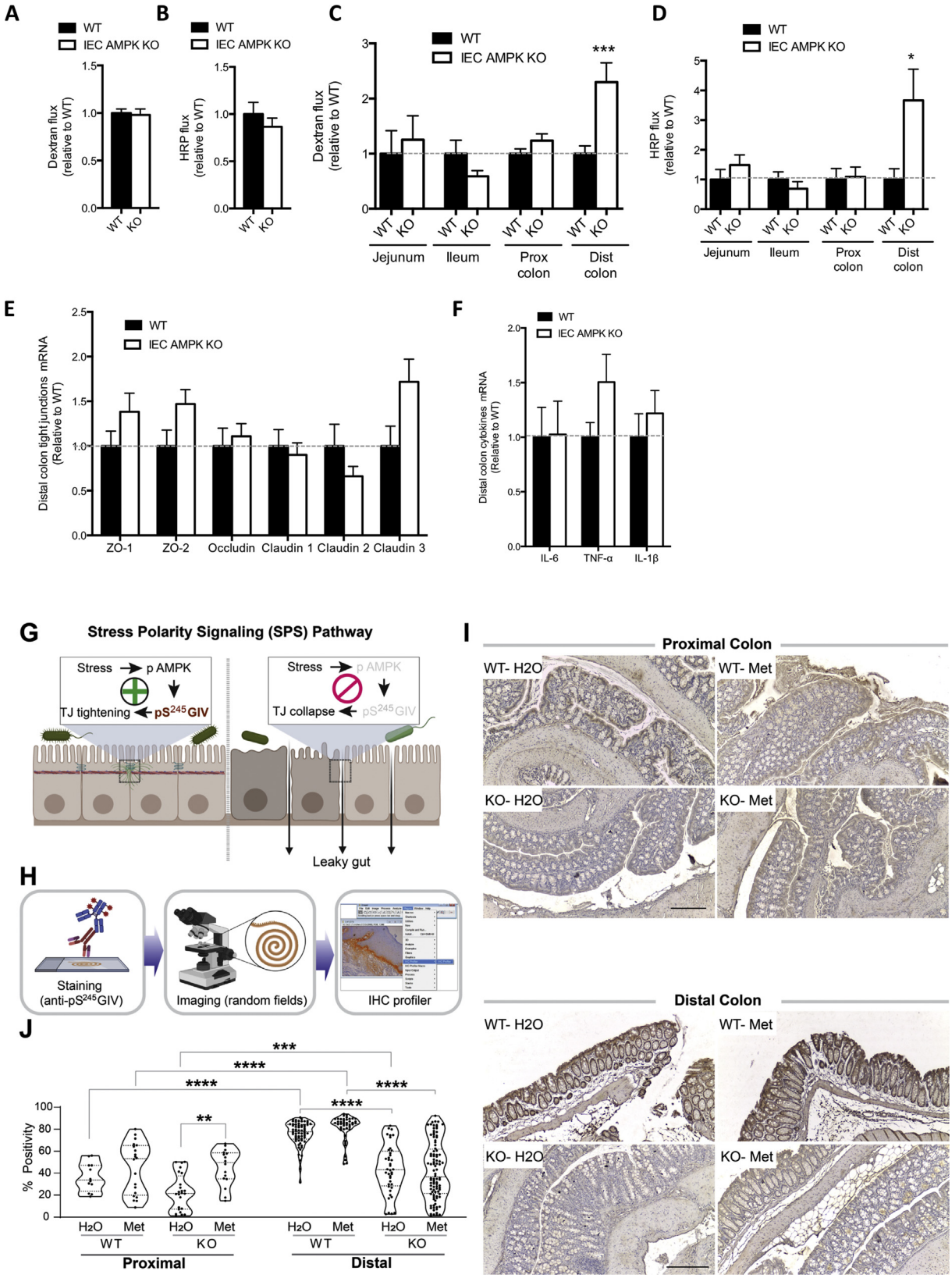


**Figure 2: Absence of IEC AMPK induced hyperpermeability in the distal colon**. (A) *In vivo* paracellular intestinal epithelial permeability of WT and IEC AMPK KO mice on regular control diet (CD) determined by measuring the amount of 4 kDa TRITC-dextran in the plasma 4 h after gavage. n = 3–7 mice per genotype from three independent experiments. (B) *In vivo* transcellular intestinal epithelial permeability of WT and IEC AMPK KO mice on CD determined by measuring the activity of HRP in the plasma 4 h after oral gavage. n = 4–6 mice from three independent experiments. (C) *Ex vivo* paracellular permeability in the jejunum, ileum, proximal colon, and distal colon from WT and IEC AMPK KO mice on CD evaluated in Ussing chambers by measuring FITC-dextran flux through intestinal segments for 3 h. n = 7 mice. Statistical analysis was performed using Student's t

 

documented [63]. While AMPKα1 expression levels did not reliably change, AMPKα2 displayed a decreasing gradient of expression from the villus tips to the crypt, resulting in a two-fold AMPKα1-to-AMPKα2 expression ratio in the crypt compartment (Suppl. Figure 1A and B). To determine whether in response to the downregulation of one of the AMPKα catalytic subunits upregulation of the remaining subunits could occur in the intestine as previously reported in skeletal muscle, kidney, or intestinal epithelial Caco-2 cells [23,53,64], we examined the expression of AMPKα1 and AMPKα2 in IECs isolated from the global AMPKα1 KO and global AMPKα2 KO mice. Absence of AMPKα1 isoform was associated with increased levels of the AMPKα2 isoform and vice versa, suggesting a compensatory mechanism to maintain intestinal homeostasis (Suppl. Figure 1C). To generate mice lacking AMPK activity in the intestinal epithelium (IEC AMPK KO mice), we invalidated the two catalytic subunits of AMPK by crossing AMPKα1$^{fl/fl}$/α2$^{fl/fl}$ mice [51] with mice expressing Cre-recombinase under the control of the villin promoter, which drives the expression in the epithelium of the GI tract [52]. The development and survival of the animals were not impacted. The IEC AMPK KO mice were born in Mendelian ratios and appeared normal at birth indistinguishable from their control littermates. There was no detectable AMPKα1 and AMPKα2 expression in IECs isolated from the small and large intestines of the IEC AMPK KO mice but not the control mice (Figure 1A). AMPKα1 and AMPKα2 expression was not altered in the liver and skeletal muscle, confirming the deletion was specific to IECs (Suppl. Figure 1D). The deletion of AMPKα1 and AMPKα2 was associated with a substantial reduction in the expression of regulatory subunits AMPKβ1 and AMPKγ1, whereas the expression of AMPKβ2 and AMPKγ2 was poorly altered (Figure 1A). No changes in body weight, length of the intestine and colon, total transit time, and humidity of feces were observed in the IEC AMPK KO mice compared to the WT mice (Figure 1B–F). There was no difference in the contractile activity of the GI tract between IEC AMPK KO and WT mice (Suppl. Figure 2A and B). Necropsies revealed normal structures of the GI tract with a similar intestinal epithelial cell distribution and no sign of spontaneous colitis was observed between the IEC AMPK KO and WT mice. Hematoxylin and eosin staining or electron microscopy analysis of transverse sections of the small and large intestines showed no obvious abnormalities (Suppl. Figure 3A and B).

### 3.2. Deletion of AMPKα1 and AMPKα2 in IECs altered permeability in distal colon

To determine the role of AMPK in intestinal homeostasis, we assessed intestinal barrier permeability by measuring *in vivo* transcellular (HRP flux) and paracellular (4 kDa dextran flux) permeability. No difference was observed between the IEC AMPK KO and WT mice using *in vivo* permeability measurements (Figure 2A and B). As AMPK activation has been associated with enhanced epithelial barrier function in Caco-2 intestinal epithelial cells [23,24], we more precisely examined the impact of AMPK deletion on gut integrity by measuring *ex vivo* transcellular and paracellular permeability with different segments of the GI tract in Ussing chambers. Interestingly, the IEC AMPK KO mice displayed higher permeability exclusively in the distal colon, indicating disrupted epithelial barrier function (Figure 2C and D). However, the mRNA expression of tight junction proteins ZO-1, ZO-2, occludin, claudin 1, claudin 2, and claudin 3 did not significantly differ in entire biopsies from the distal colon (Figure 2E) and other segments of the small and large intestines (Suppl. Figure 3C) of the IEC AMPK KO and WT mice. The protein content of ZO-1 and occludin was also unaltered in the different portions of the GI tract from the IEC AMPK KO compared to the WT mice (Suppl. Figure 3D). As inflammation and IEB permeability are linked, we next analyzed whether cytokine mRNA expression was altered in the IEC AMPK KO mice (Figure 2G and Suppl. Figure 3E). While the expression of pro-inflammatory cytokines IL-6 and IL-1β was similar in the distal colon from both genotypes, TNF-α mRNA expression levels tended to be slightly increased in the absence of gut AMPK (Figure 2F).

The observed leakiness in the IEC AMPK KO distal colon was associated with the loss of a recently described polarity signaling pathway that is orchestrated by AMPK at tight junctions of the epithelial lining of the gut [28,65]. When we assessed the stress polarity signaling (SPS)-pathway using a previously validated anti-phosphoSer245 Girdin antibody [28,66], we found that the pathway was active in the WT but not IEC AMPK KO mice, specifically in the distal colon (Figure 2F–I). These findings are consistent with the fact that this pathway is triggered by microbes/microbial products that are encountered in an increasing manner in the distal colon. Taken together, these findings demonstrate that the distal colon in the IEC AMPK KO mice was leakier, and that such leakiness may at least in part be a consequence of an impaired AMPK-dependent barrier-protective pathway.

### 3.3. Constitutive intestinal AMPK deletion combined with HFD challenge did not exacerbate intestinal hyperpermeability

Obesity is associated with intestinal hyperpermeability and metabolic endotoxemia [10,67,68]. Therefore, we evaluated the effects of AMPK deletion on intestinal permeability in response to a HFD challenge for 10 weeks (Figure 3A). Neither transcellular nor paracellular permeability was changed after the HFD challenge. There were no differences in the *in vivo* transcellular (HRP flux) and paracellular (4 kDa dextran flux) permeability between the IEC AMPK KO and WT mice at completion of the HFD challenge (Figure 3B and Suppl. Figure 4A). Again, an increased permeability was observed in the distal colon of the HFD-fed IEC AMPK KO compared to the WT (Figure 3C). As previously observed for the CD, permeability in the jejunum, ileum, or proximal colon was comparable between the WT and KO animals on the HFD (Suppl. Figure 4B and C). No differences were observed in the mRNA expression of the tight junction protein ZO-1 in the intestinal epithelial layer (IEL) fraction of the distal colon from the HFD-fed IEC

test. (D) *Ex vivo* transcellular permeability in the jejunum, ileum, proximal colon, and distal colon from WT and IEC AMPK KO mice on CD evaluated in Ussing chambers by measuring the activity of HRP in the basolateral medium for 3 h. n = 7 mice. (E) Expression of mRNA for tight junction proteins ZO-1, ZO-2, occludin, claudin 1, claudin 2, and claudin 3 in entire distal colon biopsies from WT and IEC AMPK KO mice. (F) Expression of mRNA for IL-6, TNF-α, and IL-1β in entire distal colon biopsies from WT and IEC AMPK KO mice. n = 4–7 mice. All of the data are expressed as means ± SEM. Statistical analysis was performed using Student's t test. *p < 0.05 and ***p < 0.001 indicate a significant increase relative to the respective WT intestinal segment. Black bars, WT mice (WT); white bars, IEC AMPK KO mice (KO). (G) Schematic summarizing the stress polarity signaling (SPS) pathway showing the impact of AMPK activation/deletion on Ser425 GIV phosphorylation and barrier integrity. (H) Schematic diagram displays the workflow to assess the activation of the SPS pathway *in situ* in the murine colons as determined by assessing the abundance of epithelial pS245GIV. (I) Representative images are presented from the proximal colon (upper section) and distal colon (lower section) of WT (WT) and IEC AMPK KO (KO) mice without metformin treatment ($H_2O$) and after administration of 2 mg/ml of metformin in drinking water for 5 days (Met). (J) Violin plots displaying the % area and intensity of pS245 GIV staining as determined by IHC Profiler (each dot represents the average of measurements in 4 ROIs, which were assessed in 3–5 images taken from each sample; n = 3 in $H_2O$ group; n = 5 in Met group). Error bars represent SEM. Statistical significance was determined by three-way ANOVA; **p < 0.01 and ****p < 0.0001.

 

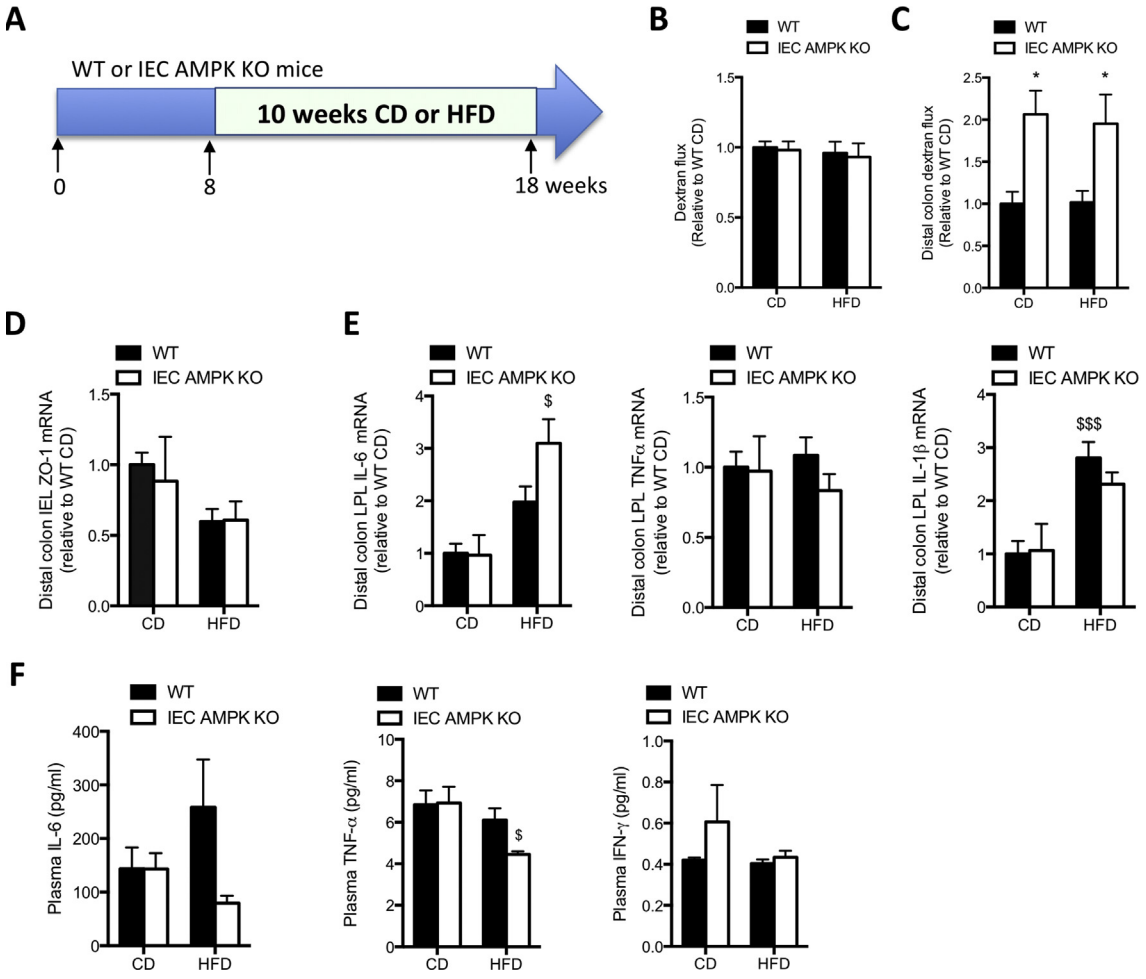


**Figure 3: Deletion of IEC AMPK did not exacerbate permeability and inflammation in the colon after a HFD challenge**. (A) Experimental timeline for control diet (CD) or high-fat diet (HFD) challenge for 10 weeks in male WT and IEC AMPK KO mice. (B) *In vivo* paracellular intestinal epithelial permeability of WT and IEC AMPK KO mice on HFD determined by measuring the amount of 4 kDa TRITC-dextran in the plasma 4 h after gavage. n = 3–7 mice from three independent experiments. (C) *Ex vivo* paracellular permeability in the distal colon of WT and IEC AMPK KO mice on a CD or HFD. Permeability was evaluated in Ussing chambers by measuring FITC-dextran flux through intestinal segments for 3 h. n = 7–12 mice. (D) Expression of mRNA for ZO-1 in the intestinal epithelial layer (IEL) fraction isolated from the distal colon of WT and IEC AMPK KO mice fed a CD or HFD. n = 7 mice. (E) Expression of mRNA for IL-6, TNF-α, and IL-1β in the lamina propria layer (LPL) fraction isolated from the distal colon of WT and IEC AMPK KO mice fed a CD or HFD. n = 7 mice. (F) Circulating IL-6, TNF-α, and IFN-γ levels in WT and IEC AMPK KO mice fed a CD or HFD. n = 5–7 mice. All of the data are expressed as mean fold change relative to WT. Statistical analysis was performed by two-way ANOVA with Bonferroni's post hoc test. *p < 0.05 and **p < 0.01 indicate a significant difference in respective WT intestinal segment and diet challenge. $p < 0.05 and $$$p < 0.001 indicate diet effect within genotype. CD, control diet; HFD, high-fat diet; black bars, WT mice; white bars, IEC AMPK KO mice.

AMPK KO and WT mice (Figure 3D). While the mRNA expression of pro-inflammatory cytokines TNF-α and IL-1β was unchanged in the lamina propria layer (LPL) of distal colon from the HFD-fed IEC AMPK KO and WT mice, there was a significant increase in IL-6 mRNA levels induced by the gut AMPK disruption (Figure 3E), suggesting alterations in the control of intestinal inflammation in the IEC AMPK KO mice fed the HFD. However, there was no difference in circulating IL-6, TNF-α, and IFN-γ levels between the IEC AMPK KO and WT mice fed the CD or HFD (Figure 3F).

### 3.4. Constitutive intestinal AMPK deletion did not exacerbate obesity-induced metabolic dysfunctions

To address whether a lack of intestinal AMPK may induce metabolic dysfunction and exacerbate diet-induced obesity, we monitored changes in body weight between the IEC AMPK KO and WT mice challenged with the CD or HFD for 10 weeks (Figure 3A). During the last week of diet exposure, there was no difference in body mass or adiposity between the IEC AMPK KO and WT mice fed a regular CD, and while the HFD increased both body mass and adiposity, the IEC AMPK KO mice gained a similar amount of body weight or fat mass as the WT mice (Figure 4A and B). Consistently, no difference was observed between the genotypes for food and drink intake and spontaneous locomotor activity when the animals were fed either the regular CD or HFD (Figure 4C–E and Suppl. Figure 5A-C). We next investigated energy metabolism and found that the IEC AMPK KO mice had a similar average energy expenditure (EE) compared to the WT mice fed the CD or HFD during both the light and dark phases (Figure 4F). No significant changes in $VCO_2$, $VO_2$, and RER ($VCO_2$-to-$VO_2$ ratio) were observed during the light and dark phases between the WT and IEC AMPK KO mice fed the CD or HFD, indicating similar oxidation capacity between the genotypes (Figure 4G–I). However, a small but not significant trend (p = 0.0608) for increased RER was observed in the IEC AMPK KO

 

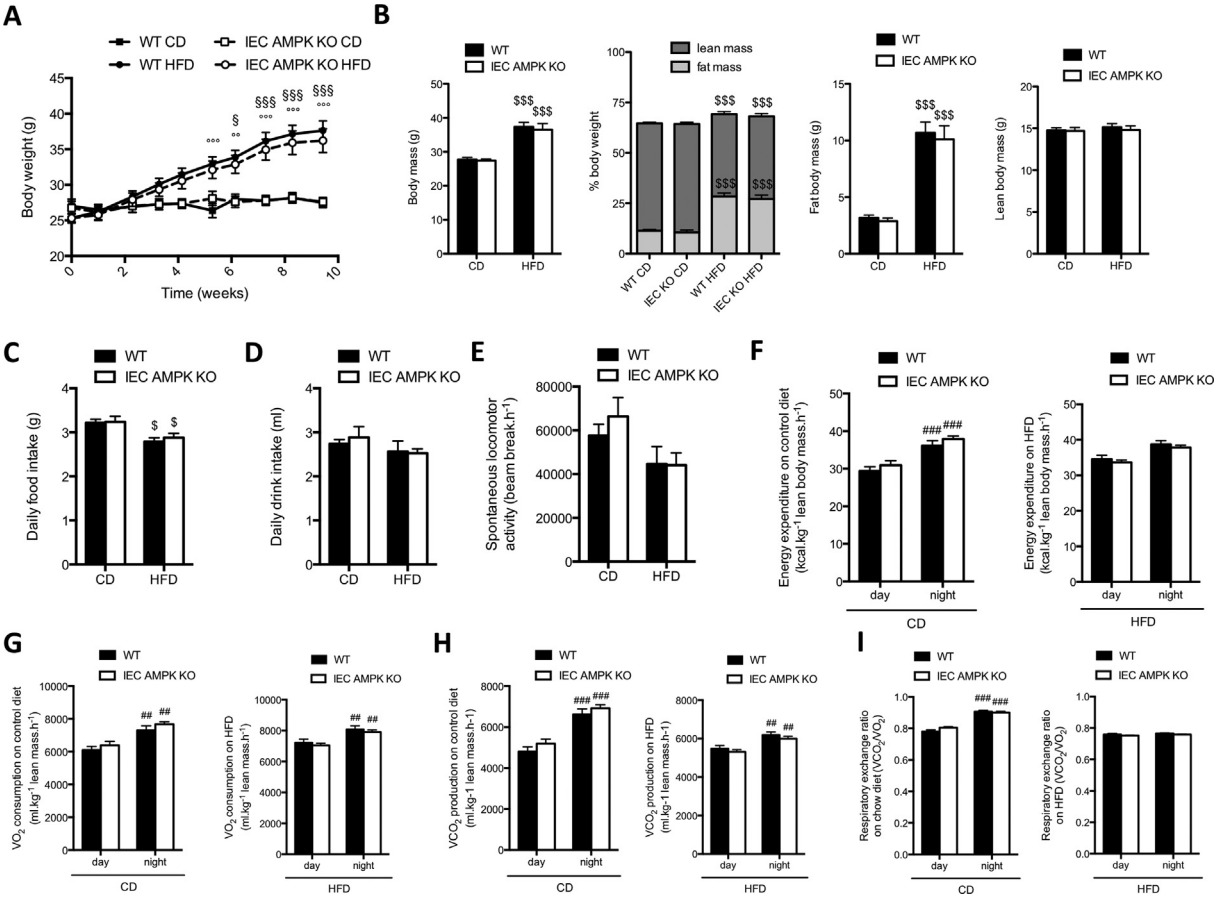


**Figure 4: Deletion of IEC AMPK did not worsen HFD-induced obesity**. (A) Body weight monitoring in WT and IEC AMPK KO mice on control diet (CD) or high-fat diet (HFD) for 10 weeks. n = 5–7 mice. (B) Body weight, body composition examination (expressed as a percentage of fat mass and lean mass relative to total body mass), body fat mass, and body lean mass measured by nuclear magnetic resonance in WT and IEC AMPK KO mice at the end of CD and HFD challenge. n = 5–7 mice. (C) Daily food intake of WT and IEC AMPK KO mice on CD or HFD. (D) Daily drink intake of WT and IEC AMPK KO mice on CD or HFD. (E) Daily spontaneous locomotor activity of WT and IEC AMPK KO mice. (F) Energy expenditure of WT and IEC AMPK KO mice on CD or HFD during the light and dark phases. (G) $O_2$ consumption of WT and IEC AMPK KO mice on CD or HFD during the light and dark phases. (H) $CO_2$ production of WT and IEC AMPK KO mice on CD or HFD during the light and dark phases. (I) Respiratory exchange ratio ($VCO_2/VO_2$) of WT and IEC AMPK KO mice fed a CD or HFD during the light and dark phases. All of the calorimetry data are representative of 5 days of measurement; n = 6 mice. All of the data are expressed as means ± SEM. Statistical analysis was performed by two-way ANOVA with Bonferroni's post hoc test. $^{00}p < 0.01$ and $^{000}p < 0.001$ indicate a diet effect in WT mice. §p < 0.05 and §p < 0.001 indicate a diet effect in IEC AMPK KO mice. $p < 0.05 and $$$p < 0.001 indicate a diet effect within genotype. ##p < 0.01 and ###p < 0.001 indicate a light/dark phase effect within genotype. CD, control diet; HFD, high-fat diet; black bars, WT mice; white bars, IEC AMPK KO mice.

mice when fed the control diet (Figure 4I). There was no difference in postprandial triglyceride clearance from the circulation during an oral fat tolerance test using an oral gavage of olive oil, indicating unaltered lipid absorption and maintenance of systemic lipid homeostasis between the WT and IEC AMPK KO mice (Suppl. Figure 5D). Plasma lipid parameters were not consistently affected by genotype in the mice fed the regular CD or HFD (Suppl. Figure 5E). Glucose tolerance and insulin sensitivity were also similar between the IEC AMPK KO and WT mice fed the CD or HFD (Figure 5A and B). The plasma GLP-1 levels were comparable in the IEC AMPK KO and WT mice in the basal state or after an oral challenge with a bolus of glucose in olive oil to stimulate GLP-1 secretion (Suppl. Figure 5F). Overall, these data indicated that the lack of AMPK in IECs did not promote or exacerbate the dysregulation of glucose homeostasis.

### 3.5. Intestinal AMPK was dispensable for the acute glucose-lowering action of metformin

Recent studies have reported that the GI tract contributes to the overall glucose-lowering effect of the anti-diabetic drug metformin [69]. Since a glucoregulatory role of AMPK activation in the duodenal mucosal layer has been demonstrated in response to an infusion of metformin into the gut [70], we evaluated the improvement in glucose tolerance after oral dosing with metformin. Treating the WT mice fed the CD or HFD with a single dose of 250 mg/kg metformin was capable of consistently lowering glucose excursions during oral glucose tolerance tests but removing IEC AMPK was ineffective on the glucose-lowering ability of metformin, indicating that the acute glycemic control by metformin was conferred independently of intestinal AMPK. (Figure 5C and D).

### 3.6. Inducible intestinal AMPK deletion did not impact obesity-induced metabolic dysfunctions

To investigate whether intestinal AMPK could shape the gut microbiota, we analyzed changes in microbiota composition in response to the HFD in mice lacking IEC AMPK. To circumvent potential effects of AMPK removal on microbiota composition prior to the HFD challenge, we generated an inducible deletion of both AMPK$\alpha$1 and AMPK$\alpha$2 in IECs by crossing AMPK$\alpha1^{fl/fl}/\alpha2^{fl/fl}$ mice with transgenic mice expressing

 

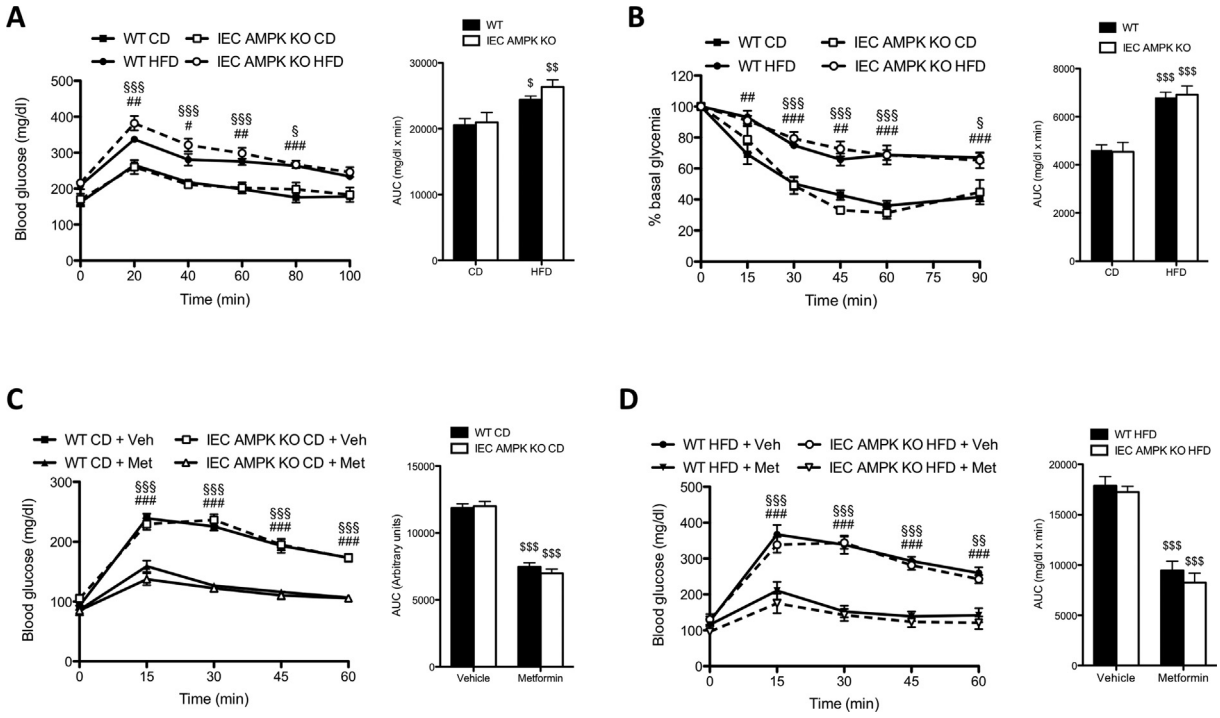


**Figure 5: Deletion of IEC AMPK did not worsen obesity-induced metabolic dysfunctions and did not affect the acute response to metformin**. (A) Blood glucose profile during glucose tolerance test in WT and IEC AMPK KO mice on control diet (CD) or high-fat diet (HFD). AUC, area under the curve was calculated. n = 5–7 mice. (B) Blood glucose profile during insulin tolerance tests in WT and IEC AMPK KO mice on CD or HFD. n = 5–7 mice. (C) Blood glucose profile during metformin tolerance tests in WT and IEC AMPK KO mice on CD. Mice were given an oral gavage dose of 250 mg/kg of metformin and after 30 min challenged with an oral administration of glucose. n = 7–8 mice per genotype. (D) Blood glucose profile during metformin tolerance tests in WT and IEC AMPK KO mice on HFD. Mice were given an oral gavage dose of 250 mg/kg of metformin and after 30 min challenged with an oral administration of glucose. n = 5–7 mice. All of the data are expressed as means ± SEM. Statistical analysis was performed by two-way repeated measures ANOVA or two-way ANOVA with Bonferroni's post hoc test. Black bars, WT mice; white bars, IEC AMPK KO mice. ##p < 0.01 and ###p < 0.001 indicate a diet or metformin effect in WT mice. §p < 0.05, §§p < 0.01, and §§§p < 0.001 indicate a diet or metformin effect in IEC AMPK KO mice. $p < 0.05, $$p < 0.01, and $$$p < 0.001 indicate a diet or metformin effect within genotype. CD, control diet; HFD, high-fat diet; black bars, WT mice; white bars, IEC AMPK KO mice.

tamoxifen-dependent Cre recombinase (Cre-ERT2) under the control of the villin promoter [52]. After tamoxifen treatment, the i-IEC AMPK KO mice displayed no detectable AMPK$\alpha$1 and AMPK$\alpha$2 expression in IECs isolated from small and large intestinal segments (Suppl. Figure 6A). We next evaluated the effects of the inducible deletion of intestinal AMPK at weaning prior to a challenge with a CD or HFD for 16 weeks (Figure 6A). At the end of the diet intervention, we checked that there was no more detectable AMPK$\alpha$1 and AMPK$\alpha$2 expression in IECs isolated from the GI tract of the i-IEC AMPK KO and WT mice (Figure 6B). Body weight gain and adiposity were similar in both genotypes fed either the regular CD or HFD (Figure 6C and D and Suppl. Figure 6B). These findings were consistent with the absence of differences in macrophage, neutrophil, dendritic cell, and monocyte numbers in the visceral adipose tissue of the i-IEC AMPK KO and WT mice fed the CD or HFD (Suppl. Figure 6C). There was also no difference in overall glucose excursion during oral glucose tolerance tests between the i-IEC AMPK KO and WT mice fed the CD or HFD (Figure 6E).

### 3.7. Inducible intestinal AMPK deletion modulated the composition of gut microbiota in CD- but not HFD-fed mice

We collected stool samples from the WT and i-IEC AMPK KO mice fed the CD or HFD for 16 weeks and the fecal microbiota composition was analyzed by 16S rRNA gene-based sequencing. Principal coordinate analysis (PCoA) based on unweighted UniFrac-based distances showed a clear separation between gut communities in the CD- and HFD-fed mice (Figure 7A). Likewise, the Shannon $\alpha$-diversity of gut microbiota was slightly increased in the HFD-fed mice (Figure 7B). Results from *t* tests showed that the average Shannon indices were significantly different between the CD-fed WT mice and WT and i-IEC AMPK KO mice on the HFD (p values of 0.012 and 0.021, respectively) (Figure 7B). Interestingly, the gut microbiota composition was substantially altered in the CD-fed i-IEC AMPK KO mice compared to the CD-fed WT mice but the difference was lost when the i-IEC AMPK KO and WT mice were fed the HFD (Figure 7C). In accordance with the PCoA results, the relative abundance of bacterial orders in each group highlighted the impact of the HFD on gut microbiota and the differences between the WT and i-IEC AMPK KO mice fed the CD. We found that the percentages of *Clostridiales* and *Desulfovibrionales* seemed enriched in the CD-fed i-IEC AMPK KO mice, whereas the CD-fed WT mice showed increased proportions of *Erysipelotrichales* (Figure 7C). Challenge with the HFD induced an increase in *Clostridiales* and *Lactobacillales* and a decrease in *Bacteroidales* and *Bifidobacteriales*. However, we did not observe major differences between microbiota in the WT and i-IEC AMPK KO mice under the HFD, except a decrease in *Verrucomicrobiales* in the i-IEC AMPK KO mice (Figure 7C). We analyzed then the gut microbiota at a deeper taxonomic (genus) level and identified individual taxa modulated selectively in the different groups of mice (Figure 7D). We next used the linear discriminant analysis (LDA) effect size (LEfSe) to examine statistical differences in the relative abundance of gut microbiota between genotypes. By selecting strong associations in the LDA (LDA scores > 3), we showed

 

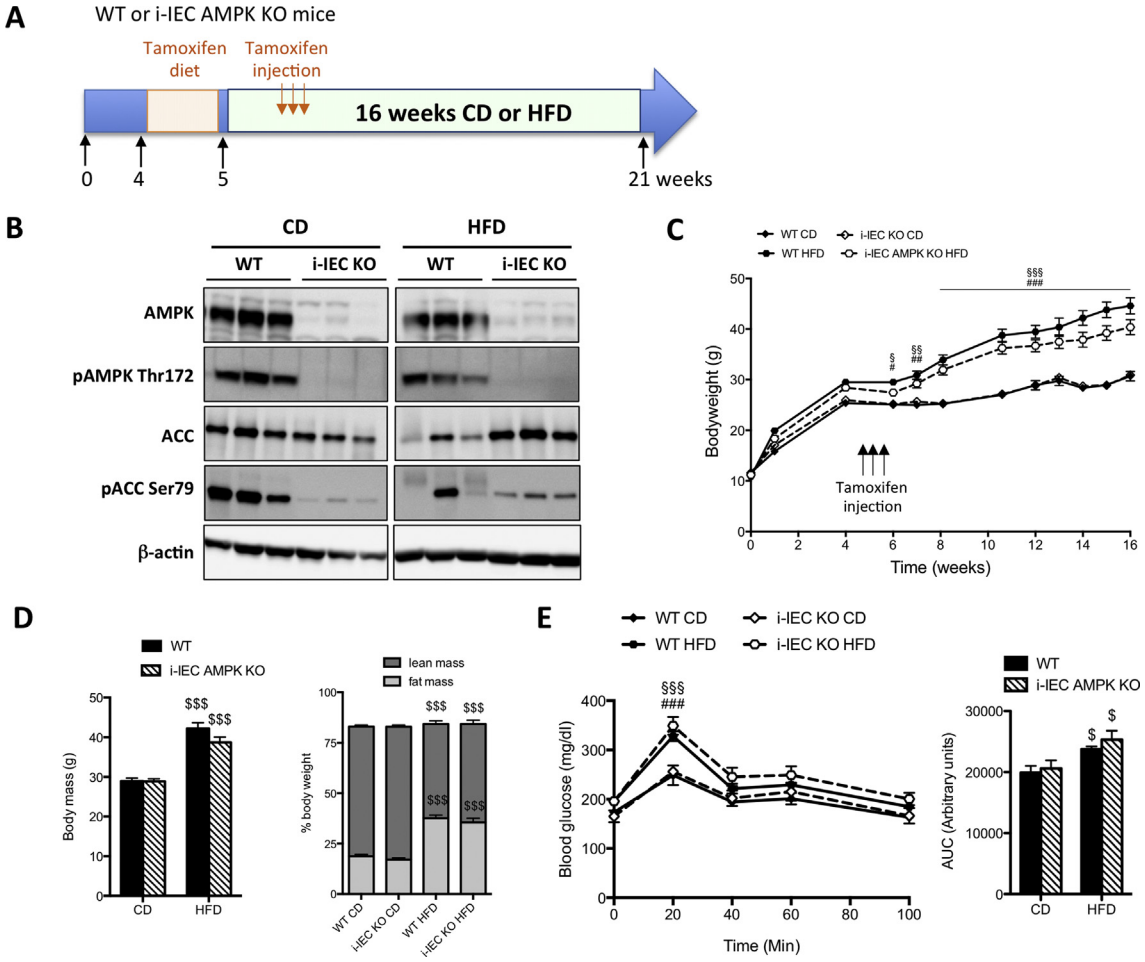


**Figure 6: Inducible deletion of gut AMPK did not exacerbate the development of HFD-induced obesity and metabolic dysfunctions**. (A) Experimental timeline for tamoxifen treatment and control diet (CD) or high-fat diet (HFD) challenge for 16 weeks in male WT and i-IEC AMPK KO mice. (B) Western blotting analysis of AMPKα, phospho-AMPKα-Thr172, ACC, and phospho-ACC-Ser79 expression in intestinal epithelial cells isolated from the ileum of WT and i-IEC AMPK KO mice at the completion of CD or HFD challenge. β-actin was used as a loading control. (C) Body weight monitoring in WT and i-IEC AMPK KO mice on CD or HFD for 16 weeks. n = 7–13 mice. (D) Body weight and body composition examination (expressed as a percentage of fat mass and lean mass relative to total body mass) in WT and i-IEC AMPK KO mice at the end of CD or HFD challenge. n = 7–13 mice. (E) Blood glucose profile during glucose tolerance tests in WT and i-IEC AMPK KO mice on CD or HFD. AUC, area under the curve was calculated. n = 6–11 mice. All of the data are expressed as means ± SEM. Statistical analysis was performed by two-way repeated measures ANOVA or two-way ANOVA with Bonferroni's post hoc test. ##p < 0.01 and ###p < 0.001 indicate a diet effect in WT mice. §§p < 0.01 and §§§p < 0.001 indicate a diet effect in i-IEC AMPK KO mice. $p < 0.05 and $$$p < 0.001 indicate a diet effect within genotype. CD, control diet; HFD, high-fat diet; black bars, WT mice; dashed bars, i-IEC AMPK KO mice.

that *Parasutterella* and *Parvibacter* were more abundant in the WT mice under the CD whereas *GCA-900066225*, *Dubosiella*, *Roseburia*, *Anaerovorax*, *Alloprevotella*, *Enterorhabdus*, *Desulfovibrionaceae*, and genera from the *Clostridiales* order and the *Lachnospiraceae-NK4A136* group were more abundant in the i-IEC AMPK KO mice (Figure 7E). Unlike the CD-fed mice, the bacterial composition was very similar between the WT and i-IEC AMPK KO mice fed the HFD. We could however notice an increase of *Parvibacter* in the WT mice and, interestingly, the abundance of *Akkermansia*, well known for improving gut barrier function [71], decreased in the i-IEC AMPK KO mice (Figure 7F).

### 3.8. Inducible deletion of intestinal AMPK did not worsen obesity-induced hyperpermeability

We next determined if inducible deletion of intestinal AMPK influenced intestinal integrity in the same manner following constitutive deletion. The *in vivo* paracellular permeability (4 kDa dextran flux) was similar between the WT and i-IEC AMPK KO mice fed the regular CD or HFD (Figure 8A). In contrast, measurement of *ex vivo* paracellular permeability revealed a dramatic increase in permeability in the distal colon from the i-IEC AMPK KO mice fed the regular CD but not when challenged with the HFD (Figure 8B). Of note, intestinal permeability was not different in the jejunum from the i-IEC AMPK KO and WT mice fed the CD or HFD (Suppl. Figure 6D). Expression levels of pro-inflammatory cytokines IL-6 and TNF-α were also similar in the distal colon from the WT and i-IEC AMPK KO mice fed the CD or HFD but the IL-1β levels were slightly decreased in the i-IEC AMPK KO mice fed the HFD (Figure 8D). Accordingly, fecal Lcn-2 levels, a sensitive and broadly dynamic marker of intestinal inflammation [59], were not different between genotypes on the CD or HFD (Figure 8E). There were also no differences in the percentage of macrophages and monocytes among $CD45^+$ cells in the colon from the i-IEC AMPK KO and WT mice fed the CD or HFD (Suppl. Figure 6E). Measurement of circulating IL-6, TNF-α, and IFN-γ levels revealed no difference between genotypes on the CD or HFD (Figure 8F). Expression levels of the tight junction protein occludin were unchanged in the distal colon from the WT and i-

 

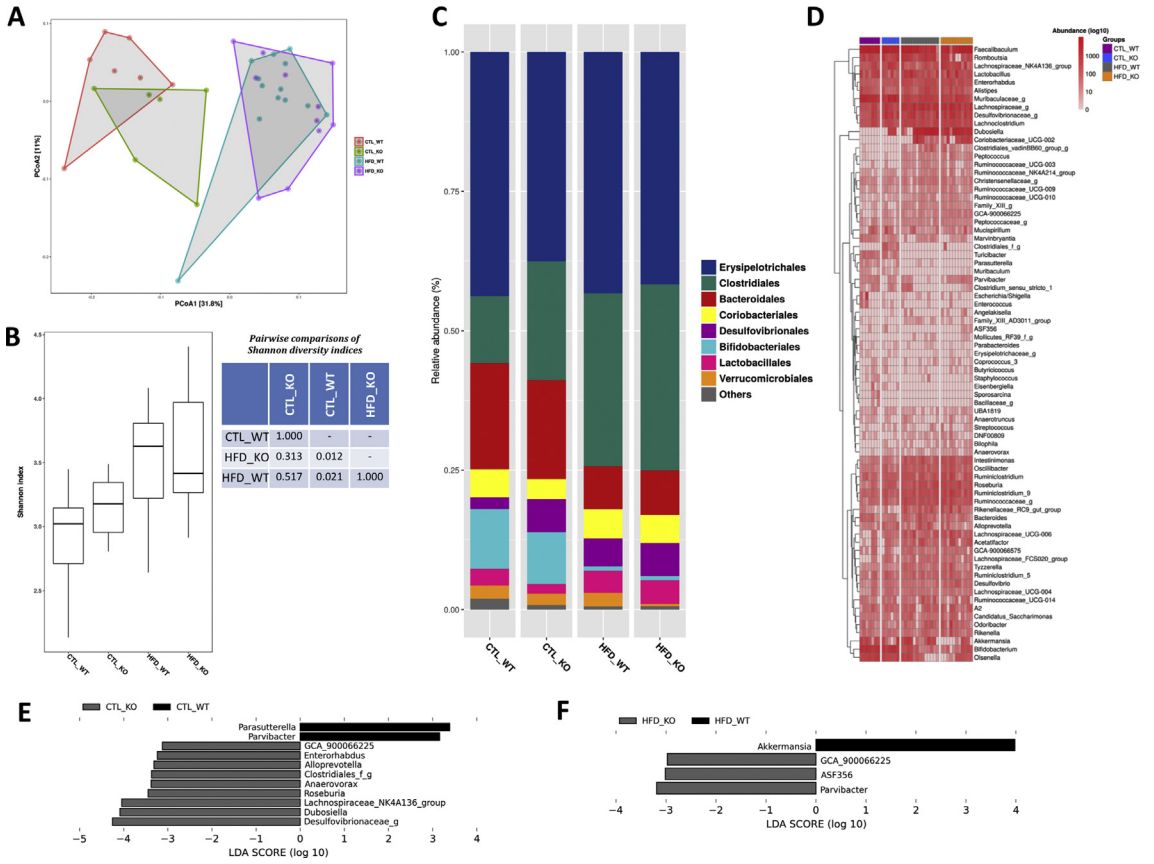


**Figure 7: Effect of inducible deletion of IEC AMPK on gut microbiota in mice on CD and HFD**. (A) Principal coordinate analysis (PCoA) based on the unweighted UniFrac distance between samples from WT and i-IEC AMPK KO mice on control diet (CD) and high-fat diet (HFD). (B) The Shannon index representing $\alpha$ diversity of microbial communities of WT and i-IEC AMPK KO mice on CD and HFD. Box plots for each $\alpha$ diversity metric and pairwise comparisons between the groups using t tests with pooled SD and Bonferroni's correction are shown. (C) Relative abundance of bacterial orders in WT and i-IEC AMPK KO mice on CD and HFD. (D) Heat map of bacterial genera abundance in each subgroup. The color scale represents the $\log_{10} + 1$ transformed abundance. "_f" or "_g" at the end of taxon name indicate unidentified families or genera, respectively. Linear discriminant analysis (LDA) effect size (LEfSe) score was calculated to evaluate bacterial families or genera overrepresented between WT and i-IEC AMPK KO mice on CD (E) or high-fat (F) diet. n = 7–13 mice. CTL_WT: CD-fed WT mice; CTL_KO: CD-fed i-IEC AMPK KO mice; HFD_WT: HFD-fed WT mice; HFD_KO: HFD-fed i-IEC AMPK KO mice. Black bars, WT mice; gray bars, i-IEC AMPK KO mice.

IEC AMPK KO mice fed the CD or HFD but those of ZO-1 were slightly decreased in the i-IEC AMPK KO mice (Figure 8G). Taken together, these data indicated that while inducible AMPK deletion altered gut barrier integrity in the distal colon in the CD-fed i-IEC AMPK KO mice, the HFD challenge seemed to blur the impact of the lack of intestinal AMPK.

## 4. DISCUSSION

While the GI tract is of growing therapeutic interest, little information exists on the expression and distribution of AMPK in the small and large intestines. Previous studies reported the predominance of AMPK$\alpha$1 catalytic isoform expression in human colon carcinoma Caco2 cells [23,72]. We showed that both catalytic isoforms AMPK$\alpha$1 and AMPK$\alpha$2 were expressed along the mouse GI tract following an antero-posterior gradient. The observation that AMPK$\alpha$2 over-expression compensated for the loss of AMPK$\alpha$1 in the GI tract of the AMPK$\alpha$1 KO mice, and vice versa, led us to generate a mouse model without intestinal AMPK activity by deleting both AMPK$\alpha$1 and AMPK$\alpha$2 catalytic subunits. Although this mouse model did not permit us to analyze the catalytic isoform-specific contributions, we cannot exclude that intestinal AMPK$\alpha$1- and AMPK$\alpha$2-containing heterotrimers have different phosphorylation targets and functions. Recent studies reported that mice harboring an intestinal-specific ablation of AMPK$\alpha$1 display impairment in intestinal barrier function, epithelial differentiation, and long-chain fatty acid uptake [24,73], indicating the absence of AMPK$\alpha$2 isoform signaling redundancy in this context. Furthermore, the antero-posterior graded distributions of the various catalytic and regulatory AMPK isoforms suggested diverse functional roles serving different physiological means to regulate GI homeostasis. Hence, further work is warranted to elucidate potential AMPK isoform-specific roles along the GI tract.

Using loss-of-function approaches, we reported that AMPK is necessary for controlling paracellular permeability in the distal colon based on an analysis in Ussing chambers. Correctly establishing cell–cell contact is crucial to maintain epithelial barrier function. The integrity of apical junctional organization, including tight junctions (TJs) and adherens junctions (AJs), plays a major role in determining mucosal permeability and its disturbance leads to leaky gut [74]. It was first demonstrated that AMPK contributes to the assembly of epithelial TJs in renal MDCK cells [17,18]. These findings were extended in intestinal cell lines, where AMPK activation was shown to promote TJ assembly associated with enhanced ZO-1 and occludin redistribution and decreased paracellular permeability [22–24,43,75]. Multiple AMPK

 

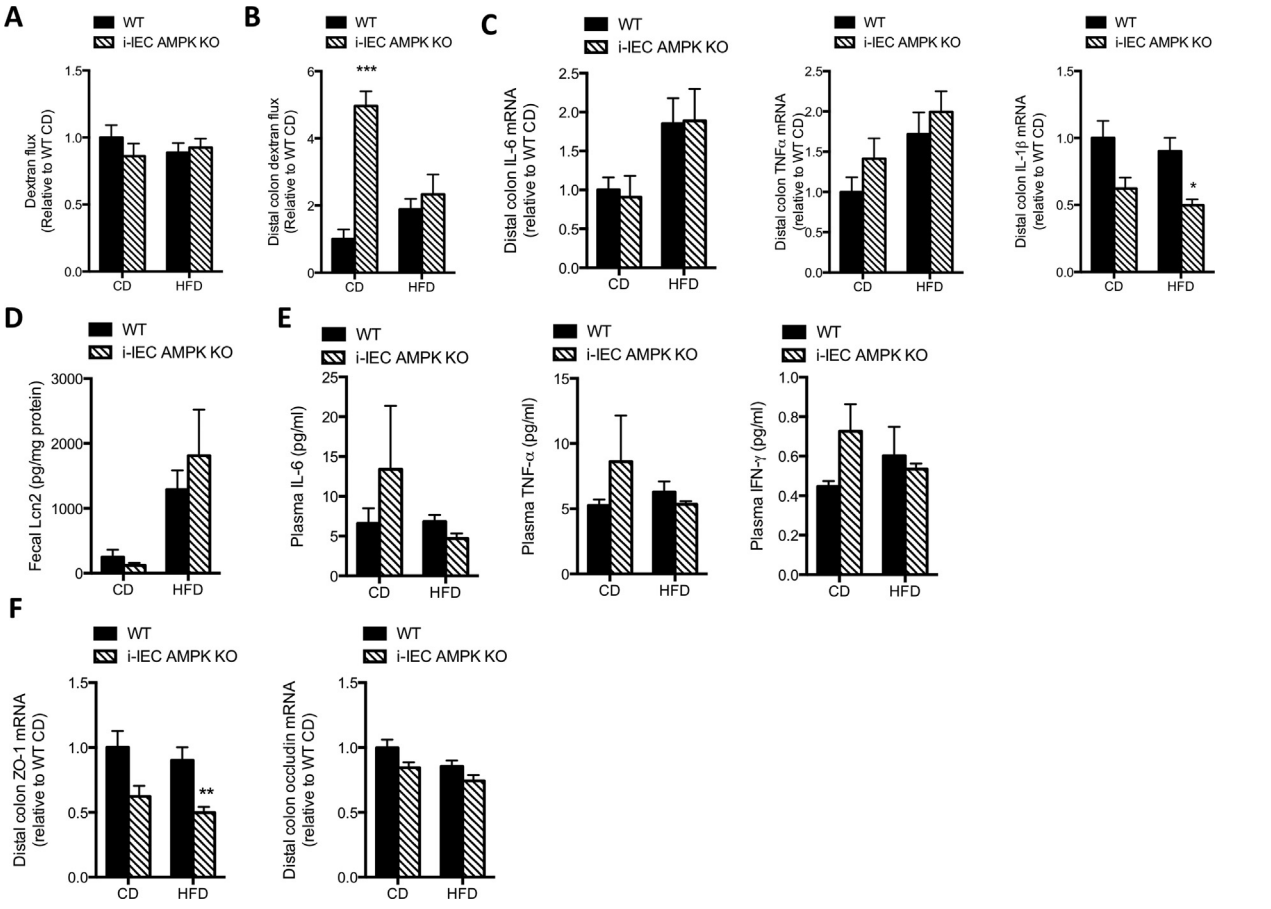


**Figure 8: Inducible deletion of intestinal AMPK did not worsen obesity-induced permeability and inflammation in the colon**. (A) *In vivo* paracellular intestinal epithelial permeability of WT and i-IEC AMPK KO mice on control diet (CD) or high-fat diet (HFD) determined by measuring the amount of 4 kDa TRITC-dextran in the plasma 4 h after gavage. n = 7–13 mice. (B) *Ex vivo* paracellular permeability in the distal colon from WT and i-IEC AMPK KO mice on CD or HFD evaluated in Ussing chambers by measuring TRITC-dextran flux through intestinal segments for 3 h. n = 3–6 mice. (C) Expression of mRNA for IL-6, TNF-α, and IL-1β in the distal colon of WT and i-IEC AMPK KO mice on CD or HFD. n = 6–13 mice. (D) Lipocalin-2 (Lcn-2) levels in feces from WT and i-IEC AMPK KO mice on CD or HFD. n = 4–10 mice. (E) Circulating IL-6, TNF-α, and IFN-γ levels in WT and i-IEC AMPK KO mice on CD or HFD. n = 3–6 mice (F) Expression of mRNA for ZO-1 and occludin in the distal colon of WT and i-IEC AMPK KO mice on CD or HFD. n = 6–13 mice. All of the data are expressed as means ± SEM. Statistical analysis was performed by two-way ANOVA with Bonferroni's post hoc test. *$p < 0.05$, **$p < 0.01$, and ***$p < 0.001$ indicate a significant increase in dextran flux relative to the respective WT intestinal segment and diet challenge. CD, control diet; HFD, high-fat diet; black bars, WT mice; dashed bars, i-IEC AMPK KO mice.

effectors known to participate in apical junction formation and assembly have been described. It was found that AMPK-modulated paracellular permeability is associated with increased protein content of claudin 1, claudin 4, occludin, and ZO-1 at TJs [19,76,77]. It was also reported that AMPK directly phosphorylates claudin 4, leading to enhanced interaction with occludin [77]. However, we noticed no relevant modifications in TJ protein expression and distribution at the plasma membrane in the distal colon lacking AMPK. It was proposed that AMPK-induced TJ assembly is mainly regulated by effectors of AMPK that orchestrate interactions between apical junctions and the cytoskeleton. A role of AMPK in regulating the association of TJs with the cytoskeletal microtubule network has been demonstrated with the direct phosphorylation of the scaffold protein cingulin on multiple residues [29,30]. Other studies suggested that AMPK activation might facilitate TJ assembly by phosphorylating afadin and inducing its association with ZO-1 [78]. Furthermore, phosphorylation of the multimodular polarity scaffold G-alpha interacting vesicle-associated (GIV) protein or Girdin by AMPK at Ser245 also participates in protecting epithelial integrity by stabilizing TJs [66]. We recently used a "gut-in-a dish" model system consisting of polarized enteroid-derived monolayers (EMDs) from mouse colon to confirm that Girdin Ser245 phosphorylation was abolished in AMPK-null compared to WT EMDs treated with the pharmacologic AMPK activators metformin and A-769662 [28]. We also demonstrated that AMPK-null EMDs display impaired barrier integrity with reduced trans-epithelial electrical resistance (TEER) in association with the loss of Girdin Ser245 phosphorylation [28]. In the present work, we showed that the SPS pathway is suppressed as determined by decreased Girdin Ser245 phosphorylation in the distal but not proximal colon of the IEC AMPK KO mice. Thus, these findings raise the possibility that Girdin may serve as one of the effectors of AMPK at the TJs.

Recent studies have suggested that intestinal hyperpermeability has a pivotal role in HFD-induced body weight gain and fat mass development [10]. However, although loss of IEC AMPK induces alteration in distal colon permeability, we observed absolutely no difference in adiposity or energy expenditure after the HFD challenge between the genotypes. This was consistent with the absence of higher systemic inflammation and similar increased macrophage infiltration into the adipose tissue in the HFD-fed mice lacking IEC AMPK. These data suggest that alterations in distal colon permeability caused by AMPK

 

deletion are not sufficient to exacerbate HFD-induced obesity and metabolic endotoxemia.

It is now widely accepted that the GI tract plays a determinant role in regulating glucose homeostasis. The gut is an important endocrine organ that secretes from specialized enteroendocrine cells distributed along the GI tract an array of gastrointestinal hormones that regulate gastric emptying, appetite, and postprandial glucose metabolism. The beneficial effects of metabolic surgery, such as Roux-en-Y gastric bypass surgery (RYGB), to reduce hyperglycemia and enhance insulin secretion independently of weight loss have highlighted the potential of gut signal modulation in the amelioration of type 2 diabetes [79,80]. While deletion of both AMPK$\alpha$1 and $\alpha$2 from intestinal enteroendocrine L cells has been shown to restrict GLP-1 secretion and induce glucose intolerance [81], we report that the absence of AMPK$\alpha$1 and $\alpha$2 in the intestinal mucosal layer has no effect on GLP-1 release and IEC AMPK KO mice display similar glucose tolerance compared to WT mice under CD or HFD feeding. The reasons for the apparent discrepancy is the use of a mouse genetic model with AMPK deletion in both intestinal enteroendocrine L cells and pancreatic $\alpha$ cells in earlier studies [81]. Inactivation of AMPK in pancreatic $\alpha$ cells may lead to compensatory adaptation of enteroendocrine L cell function as reported in the cross-talk between islet and intestine endocrine cells to preserve glucose homeostasis during the development of obesity [82].

Clinical evidence suggests that the anti-diabetic effects of metformin, a successful diabetes type 2 drug, likely originate from its actions in the gut involving gastrointestinal hormone signaling, bile acid pools, gut microbiota, and the gut—brain axis [69]. However, a major controversy concerns metformin's mode of action encompassing both AMPK-dependent and -independent mechanisms. Using IEC AMPK KO mice under CD or HFD feeding, we questioned the contribution of intestinal AMPK to the pharmacological outcomes of metformin treatment. We show that intestinal AMPK is not necessary for improved glucose tolerance using acute metformin administration. Although a duodenal AMPK-dependent pathway is involved in metformin's glucose-lowering effects [70], the differences between the present and earlier studies may result from the experimental settings (measurement of glucose tolerance vs glucose production). Alternatively, the pleiotropic properties of metformin independent of AMPK signaling may mask the AMPK-dependent metformin action in the regulation of glucose homeostasis [83].

It was previously reported that SCFAs produced by bacterial fermentation of non-digestible dietary fibers can activate AMPK and contribute to tight junction assembly in Caco-2 cells [22,43]. Recent studies further highlighted an interesting link between gut microbiota composition and AMPK activity [41,84]. In the present work, we studied the impact of IEC AMPK deletion on gut microbiota composition using an inducible model to avoid potential compensatory mechanisms caused by AMPK deletion during development. In the i-IEC AMPK KO mice fed a CD, we found a shift in the community of intestinal microbes, demonstrating the impact of host intestinal epithelial AMPK on the composition of gut microbiota. Supporting our observations, it was recently reported that high-fiber diet changes in the microbial diversity and composition (higher proportions of *Akkermansia* and *Bifidobacterium*) were lost when AMPK was inhibited via supplementation of the non-specific AMPK inhibitor Compound C in drinking water [85]. Of note, the higher abundance of the *Desulfovibrionaceae* family in the i-IEC AMPK KO mice correlated with altered barrier function in the distal colon. In accordance with these findings, mice and human patients with ulcerative colitis, a disease associated with altered intestinal permeability, showed a high proportion of *Desulfovibrionaceae* [86,87]. It is speculated that intestinal sulfate-reducing bacteria from the *Desulfovibrionaceae* family reduce mucosal thickness and facilitate contact between bacterial antigens and the mucosal immune system [87]. Other specific species (for example, *Clostridiales, Dubosiella*, *Roseburia*, *Alloprevotella*, *Enterorhabdus*, and *Anaerovorax*) discriminating the gut microbiota composition between the WT and i-IEC AMPK KO mice were also identified but the association with the pathological host status remains to be further investigated. In contrast, under HFD feeding, not much difference in the relative abundance of bacterial orders was observed between the WT and i-IEC AMPK KO mice. Likewise, the long-term HFD intake induced the same shift in microbiota populations in both the WT and i-IEC AMPK KO mice, indicating comparable obesity-related gut dysbiosis between genotypes. This may explain why the difference in paracellular permeability in the distal colon observed in the WT and i-IEC AMPK KO fed a CD was totally abolished when these mice were fed the HFD for 16 weeks. In addition, although we noticed a lower abundance of *Akkermansia* [37,71] in the HFD-fed i-IEC AMPK KO mice, this was not accompanied by increased body weight gain or metabolic dysfunction. Thus, the influence of the HFD on gut microbiota and metabolic dysfunctions appeared to be dominant over the alteration of distal colon permeability resulting from the exclusive loss of intestinal AMPK.

## 5. CONCLUSIONS

Altogether, our data support a role of intestinal AMPK in maintaining gut homeostasis under homeostatic and pathological conditions. However, we found that intestinal AMPK was not required for the regulation of glucose homeostasis or the metformin glucose-lowering effect. In particular, we found that intestinal AMPK participates in controlling intestinal integrity and permeability, specifically in the distal colon, by acting on the maintenance of barrier function. Our results suggested that blunted pSer245 GIV phosphorylation in the absence of AMPK may contribute to altered colon permeability. Our results also highlight the interactions between gut microbiota and host intestinal AMPK but fecal transfer experiments are warranted to confirm the relevance of the observed shift in bacterial species. In future studies, it will be interesting to examine whether targeting AMPK signaling via pharmacological and nutritional approaches may lead to new therapeutic avenues for leaky gut syndrome.

## AUTHOR'S CONTRIBUTION

**Séverine Olivier**: Conceptualization, data curation, formal analysis, investigation, methodology, and wrote the original draft. **Camille Pochard**: Conceptualization, data curation, formal analysis, investigation, methodology, and wrote the original draft. **Hanna Diounou**: Investigation. **Vanessa Castillo**: Investigation and methodology. **Jordane Divoux**: Investigation and methodology. **Joshua Alcantara**: Investigation and methodology. **Jocelyne Leclerc**: Investigation and methodology. **Sandra Guilmeau**: Investigation, review, and editing. **Camille Huet**: Investigation. **Wafa Charafi**: Investigation. **Thibault V. Varin**: Software and formal analysis, review, and editing. **Noëmie Daniel**: Formal analysis, investigation, methodology, review, and editing. **Marc Foretz**: Funding acquisition, investigation, methodology, resources, writing, review, and editing. **Michel Neunlist**: Funding acquisition, writing, review, and editing. **Benoit L. Salomon**: Formal analysis, funding acquisition, writing, review, and editing. **Pradipta Ghosh**: Formal analysis, funding acquisition, writing, review, and editing. **André Marette**: Formal analysis, funding acquisition, writing, review, and editing. **Malvyne Rolli-Derkinderen**: Conceptualization, data curation, investigation, methodology, project administration,

 

resources, supervision, validation, wrote the original draft, review, and editing. **Benoit Viollet**: Conceptualization, data curation, formal analysis, funding acquisition, investigation, methodology, project administration, resources, supervision, validation, wrote the original draft, review, and editing.

## ACKNOWLEDGMENTS

The authors thank the histochemistry and histology, cellular imaging, electron microscopy, cytometry, and immunobiology facilities at Institut Cochin for their support. We thank Sophie Thenet and Doriane Aguanno (Centre de Recherche des Cordeliers, Paris, France) for the use of Ussing chambers. We thank Grahame Hardie (University of Dundee, Dundee, UK) for generously providing AMPK$\alpha$1 and AMPK$\alpha$2 antibodies. The skillful assistance of Julie Jaulin for the analysis of the contractile activity is gratefully acknowledged.

These studies were supported by grants from Inserm, CNRS, Université de Paris Descartes, Région Ile-de-France, Agence Nationale de la Recherche (ANR-17-CE15-0030 and ANR-19-CE14-0023-01), and Société Francophone du Diabète (allocation de recherche SFD-Industrie 2016 Pierre Fabre Médicament). S.O. holds a doctoral fellowship from Région Ile-de-France (CORDDIM). P.G., J.A., and V.C. were supported by the National Institutes of Health (CA238042, AI141630, and CA100768 to P.G). Work was also partly funded by the Canadian Institutes for Heart Research (CIHR) to A.M. (FDN-143247). A.M. was the recipient of a Pfizer/CIHR research Chair in the pathogenesis of insulin resistance and cardiovascular diseases.

## CONFLICT OF INTEREST

None declared.

## APPENDIX A. SUPPLEMENTARY DATA

Supplementary data to this article can be found online at https://doi.org/10.1016/j.molmet.2021.101183.

## REFERENCES

[1] Chang, J., Leong, R.W., Wasinger, V.C., Ip, M., Yang, M., Phan, T.G., 2017. Impaired intestinal permeability contributes to ongoing bowel symptoms in patients with inflammatory bowel disease and mucosal healing. Gastroenterology 153(3):723—731 e721.

[2] Vivinus-Nebot, M., Frin-Mathy, G., Bzioueche, H., Dainese, R., Bernard, G., Anty, R., et al., 2014. Functional bowel symptoms in quiescent inflammatory bowel diseases: role of epithelial barrier disruption and low-grade inflammation. Gut 63(5):744—752.

[3] Odenwald, M.A., Turner, J.R., 2013. Intestinal permeability defects: is it time to treat? Clinical Gastroenterology and Hepatology 11(9):1075—1083.

[4] Wyatt, J., Vogelsang, H., Hubl, W., Waldhoer, T., Lochs, H., 1993. Intestinal permeability and the prediction of relapse in Crohn's disease. Lancet 341(8858):1437—1439.

[5] Leech, B., McIntyre, E., Steel, A., Sibbritt, D., 2019. Risk factors associated with intestinal permeability in an adult population: a systematic review. International Journal of Clinical Practice 73(10):e13385.

[6] Ohlsson, B., Orho-Melander, M., Nilsson, P.M., 2017. Higher levels of serum zonulin may rather Be associated with increased risk of obesity and hyperlipidemia, than with gastrointestinal symptoms or disease manifestations. International Journal of Molecular Sciences 18(3).

[7] Araujo, J.R., Tomas, J., Brenner, C., Sansonetti, P.J., 2017. Impact of high-fat diet on the intestinal microbiota and small intestinal physiology before and after the onset of obesity. Biochimie 141:97—106.

[8] Cani, P.D., Amar, J., Iglesias, M.A., Poggi, M., Knauf, C., Bastelica, D., et al., 2007. Metabolic endotoxemia initiates obesity and insulin resistance. Diabetes 56(7):1761—1772.

[9] Cani, P.D., Possemiers, S., Van de Wiele, T., Guiot, Y., Everard, A., Rottier, O., et al., 2009. Changes in gut microbiota control inflammation in obese mice through a mechanism involving GLP-2-driven improvement of gut permeability. Gut 58(8):1091—1103.

[10] Cani, P.D., Bibiloni, R., Knauf, C., Waget, A., Neyrinck, A.M., Delzenne, N.M., et al., 2008. Changes in gut microbiota control metabolic endotoxemia-induced inflammation in high-fat diet-induced obesity and diabetes in mice. Diabetes 57(6):1470—1481.

[11] Tilg, H., Zmora, N., Adolph, T.E., Elinav, E., 2020. The intestinal microbiota fuelling metabolic inflammation. Nature Reviews. Immunology 20(1):40—54.

[12] Lassenius, M.I., Pietiläinen, K.H., Kaartinen, K., Pussinen, P.J., Syrjänen, J., Forsblom, C., et al., 2011. Bacterial endotoxin activity in human serum is associated with dyslipidemia, insulin resistance, obesity, and chronic inflammation. Diabetes Care 34(8):1809—1815.

[13] Lynch, S.V., Pedersen, O., 2016. The human intestinal microbiome in health and disease. New England Journal of Medicine 375(24):2369—2379.

[14] Genser, L., Aguanno, D., Soula, H.A., Dong, L., Trystram, L., Assmann, K., et al., 2018. Increased jejunal permeability in human obesity is revealed by a lipid challenge and is linked to inflammation and type 2 diabetes. The Journal of Pathology 246(2):217—230.

[15] Hardie, D.G., 2014. AMP-activated protein kinase: maintaining energy homeostasis at the cellular and whole-body levels. Annual Review of Nutrition 34:31—55.

[16] Hardie, D.G., Lin, S.C., 2017. AMP-activated protein kinase - not just an energy sensor. F1000Res 6:1724.

[17] Zhang, L., Li, J., Young, L.H., Caplan, M.J., 2006. AMP-activated protein kinase regulates the assembly of epithelial tight junctions. Proceedings of the National Academy of Sciences of the USA 103(46):17272—17277.

[18] Zheng, B., Cantley, L.C., 2007. Regulation of epithelial tight junction assembly and disassembly by AMP-activated protein kinase. Proceedings of the National Academy of Sciences of the USA 104(3):819—822.

[19] Wang, B., Wu, Z., Ji, Y., Sun, K., Dai, Z., Wu, G., 2016. L-glutamine enhances tight junction integrity by activating CaMK kinase 2-AMP-activated protein kinase signaling in intestinal porcine epithelial cells. Journal of Nutrition 146(3):501—508.

[20] Cao, S., Wang, C., Yan, J., Li, X., Wen, J., Hu, C., 2020. Curcumin ameliorates oxidative stress-induced intestinal barrier injury and mitochondrial damage by promoting Parkin dependent mitophagy through AMPK-TFEB signal pathway. Free Radical Biology and Medicine 147:8—22.

[21] Wu, W., Wang, S., Liu, Q., Shan, T., Wang, Y., 2018. Metformin protects against LPS-induced intestinal barrier dysfunction by activating AMPK pathway. Molecular Pharmaceutics 15(8):3272—3284.

[22] Elamin, E.E., Masclee, A.A., Dekker, J., Pieters, H.J., Jonkers, D.M., 2013. Short-chain fatty acids activate AMP-activated protein kinase and ameliorate ethanol-induced intestinal barrier dysfunction in Caco-2 cell monolayers. Journal of Nutrition 143(12):1872—1881.

[23] Olivier, S., Leclerc, J., Grenier, A., Foretz, M., Tamburini, J., Viollet, B., 2019. AMPK activation promotes tight junction assembly in intestinal epithelial CaCO-2 cells. International Journal of Molecular Sciences 20(20).

[24] Sun, X., Yang, Q., Rogers, C.J., Du, M., Zhu, M.J., 2017. AMPK improves gut epithelial differentiation and barrier function via regulating Cdx2 expression. Cell Death & Differentiation 24(5):819—831.

[25] Chang, K.W., Kuo, C.Y., 2015. 6-Gingerol modulates proinflammatory responses in dextran sodium sulfate (DSS)-treated Caco-2 cells and experimental colitis in mice through adenosine monophosphate-activated protein kinase (AMPK) activation. Food & Function 6(10):3334—3341.

[26] Wongkrasant, P., Pongkorpsakol, P., Ariyadamrongkwan, J., Meesomboon, R., Satitsri, S., Pichyangkura, R., et al., 2020. A prebiotic fructo-oligosaccharide

 

promotes tight junction assembly in intestinal epithelial cells via an AMPK-dependent pathway. Biomedicine & Pharmacotherapy 129:110415.

[27] Zhu, M.J., Sun, X., Du, M., 2018. AMPK in regulation of apical junctions and barrier function of intestinal epithelium. Tissue Barriers 6(2):1—13.

[28] Ghosh, P., Swanson, L., Sayed, I.M., Mittal, Y., Lim, B.B., Ibeawuchi, S.R., et al., 2020. The stress polarity signaling (SPS) pathway serves as a marker and a target in the leaky gut barrier: implications in aging and cancer. Life Science Alliance 3(3).

[29] Ducommun, S., Deak, M., Sumpton, D., Ford, R.J., Nunez Galindo, A., Kussmann, M., et al., 2015. Motif affinity and mass spectrometry proteomic approach for the discovery of cellular AMPK targets: identification of mitochondrial fission factor as a new AMPK substrate. Cellular Signalling 27(5): 978—988.

[30] Yano, T., Matsui, T., Tamura, A., Uji, M., Tsukita, S., 2013. The association of microtubules with tight junctions is promoted by cingulin phosphorylation by AMPK. The Journal of Cell Biology 203(4):605—614.

[31] Postler, T.S., Ghosh, S., 2017. Understanding the holobiont: how microbial metabolites affect human health and shape the immune system. Cell Metabolism 26(1):110—130.

[32] Cani, P.D., 2019. Microbiota and metabolites in metabolic diseases. Nature Reviews Endocrinology 15(2):69—70.

[33] Sonnenburg, J.L., Backhed, F., 2016. Diet-microbiota interactions as moderators of human metabolism. Nature 535(7610):56—64.

[34] Dosoky, N.S., May-Zhang, L.S., Davies, S.S., 2020. Engineering the gut microbiota to treat chronic diseases. Applied Microbiology and Biotechnology 104(18):7657—7671.

[35] Hiippala, K., Jouhten, H., Ronkainen, A., Hartikainen, A., Kainulainen, V., Jalanka, J., et al., 2018. The potential of gut commensals in reinforcing intestinal barrier function and alleviating inflammation. Nutrients 10(8).

[36] Hiel, S., Gianfrancesco, M.A., Rodriguez, J., Portheault, D., Leyrolle, Q., Bindels, L.B., et al., 2020. Link between gut microbiota and health outcomes in inulin -treated obese patients: lessons from the Food4Gut multicenter randomized placebo-controlled trial. Clinical Nutrition.

[37] Depommier, C., Everard, A., Druart, C., Plovier, H., Van Hul, M., Vieira-Silva, S., et al., 2019. Supplementation with Akkermansia muciniphila in overweight and obese human volunteers: a proof-of-concept exploratory study. Nature Medicine 25(7):1096—1103.

[38] Krumbeck, J.A., Rasmussen, H.E., Hutkins, R.W., Clarke, J., Shawron, K., Keshavarzian, A., et al., 2018. Probiotic Bifidobacterium strains and galactooligosaccharides improve intestinal barrier function in obese adults but show no synergism when used together as synbiotics. Microbiome 6(1):121.

[39] Donohoe, D.R., Garge, N., Zhang, X., Sun, W., O'Connell, T.M., Bunger, M.K., et al., 2011. The microbiome and butyrate regulate energy metabolism and autophagy in the mammalian colon. Cell Metabolism 13(5):517—526.

[40] Backhed, F., Manchester, J.K., Semenkovich, C.F., Gordon, J.I., 2007. Mechanisms underlying the resistance to diet-induced obesity in germ-free mice. Proceedings of the National Academy of Sciences of the USA 104(3): 979—984.

[41] Araujo, J.R., Tazi, A., Burlen-Defranoux, O., Vichier-Guerre, S., Nigro, G., Licandro, H., et al., 2020. Fermentation products of commensal bacteria alter enterocyte lipid metabolism. Cell Host & Microbe 27(3):358—375 e357.

[42] Carvalho, B.M., Guadagnini, D., Tsukumo, D.M.L., Schenka, A.A., Latuf-Filho, P., Vassallo, J., et al., 2012. Modulation of gut microbiota by antibiotics improves insulin signalling in high-fat fed mice. Diabetologia 55(10):2823—2834.

[43] Peng, L., Li, Z.R., Green, R.S., Holzman, I.R., Lin, J., 2009. Butyrate enhances the intestinal barrier by facilitating tight junction assembly via activation of AMP-activated protein kinase in Caco-2 cell monolayers. Journal of Nutrition 139(9):1619—1625.

[44] Elamin, E., Jonkers, D., Juuti-Uusitalo, K., van Ijzendoorn, S., Troost, F., Duimel, H., et al., 2012. Effects of ethanol and acetaldehyde on tight junction integrity: in vitro study in a three dimensional intestinal epithelial cell culture model. PloS One 7(4):e35008.

[45] Li, Q., Chen, H., Zhang, M., Wu, T., Liu, R., 2019. Altered short chain fatty acid profiles induced by dietary fiber intervention regulate AMPK levels and intestinal homeostasis. Food & Function 10(11):7174—7187.

[46] Bibi, S., Kang, Y., Du, M., Zhu, M.J., 2018. Dietary red raspberries attenuate dextran sulfate sodium-induced acute colitis. The Journal of Nutritional Biochemistry 51:40—46.

[47] Gai, L., Chu, L., Xia, R., Chen, Q., Sun, X., 2019. Barbaloin attenuates mucosal damage in experimental models of rat colitis by regulating inflammation and the AMPK signaling pathway. Medical Science Monitor 25:10045—10056.

[48] Wei, W., Ding, M., Zhou, K., Xie, H., Zhang, M., Zhang, C., 2017. Protective effects of wedelolactone on dextran sodium sulfate induced murine colitis partly through inhibiting the NLRP3 inflammasome activation via AMPK signaling. Biomedicine & Pharmacotherapy 94:27—36.

[49] Zhou, K., Cheng, R., Liu, B., Wang, L., Xie, H., Zhang, C., 2018. Eupatilin ameliorates dextran sulphate sodium-induced colitis in mice partly through promoting AMPK activation. Phytomedicine 46:46—56.

[50] Scharl, M., Paul, G., Barrett, K.E., McCole, D.F., 2009. AMP-activated protein kinase mediates the interferon-gamma-induced decrease in intestinal epithelial barrier function. Journal of Biological Chemistry 284(41):27952—27963.

[51] Boudaba, N., Marion, A., Huet, C., Pierre, R., Viollet, B., Foretz, M., 2018. AMPK Re-activation suppresses hepatic steatosis but its downregulation does not promote fatty liver development. EBioMedicine 28:194—209.

[52] el Marjou, F., Janssen, K.P., Chang, B.H., Li, M., Hindie, V., Chan, L., et al., 2004. Tissue-specific and inducible Cre-mediated recombination in the gut epithelium. Genesis 39(3):186—193.

[53] Viollet, B., Andreelli, F., Jorgensen, S.B., Perrin, C., Geloen, A., Flamez, D., et al., 2003. The AMP-activated protein kinase alpha2 catalytic subunit controls whole-body insulin sensitivity. Journal of Clinical Investigation 111(1):91—98.

[54] De Quelen, F., Chevalier, J., Rolli-Derkinderen, M., Mourot, J., Neunlist, M., Boudry, G., 2011. n-3 polyunsaturated fatty acids in the maternal diet modify the postnatal development of nervous regulation of intestinal permeability in piglets. Journal of Physiology 589(17):4341—4352.

[55] Anhê, F.F., Nachbar, R.T., Varin, T.V., Trottier, J., Dudonné, S., Le Barz, M., et al., 2019. Treatment with camu camu (Myrciaria dubia) prevents obesity by altering the gut microbiota and increasing energy expenditure in diet-induced obese mice. Gut 68(3):453—464.

[56] Callahan, B.J., McMurdie, P.J., Rosen, M.J., Han, A.W., Johnson, A.J., Holmes, S.P., 2016. DADA2: high-resolution sample inference from Illumina amplicon data. Nature Methods 13(7):581—583.

[57] Wang, Q., Garrity, G.M., Tiedje, J.M., Cole, J.R., 2007. Naive Bayesian classifier for rapid assignment of rRNA sequences into the new bacterial taxonomy. Applied and Environmental Microbiology 73(16):5261—5267.

[58] Quast, C., Pruesse, E., Yilmaz, P., Gerken, J., Schweer, T., Yarza, P., et al., 2013. The SILVA ribosomal RNA gene database project: improved data processing and web-based tools. Nucleic Acids Research 41(Database issue): D590—D596.

[59] Chassaing, B., Srinivasan, G., Delgado, M.A., Young, A.N., Gewirtz, A.T., Vijay-Kumar, M., 2012. Fecal lipocalin 2, a sensitive and broadly dynamic non-invasive biomarker for intestinal inflammation. PloS One 7(9):e44328.

[60] Guilmeau, S., Flandez, M., Bancroft, L., Sellers, R.S., Tear, B., Stanley, P., et al., 2008. Intestinal deletion of Pofut1 in the mouse inactivates notch signaling and causes enterocolitis. Gastroenterology 135(3):849—860, 860 e841-846.

[61] Mariadason, J.M., Nicholas, C., L'Italien, K.E., Zhuang, M., Smartt, H.J., Heerdt, B.G., et al., 2005. Gene expression profiling of intestinal epithelial cell maturation along the crypt-villus axis. Gastroenterology 128(4):1081—1088.

[62] Segata, N., Izard, J., Waldron, L., Gevers, D., Miropolsky, L., Garrett, W.S., et al., 2011. Metagenomic biomarker discovery and explanation. Genome Biology 12(6):R60.

 

[63] Moor, A.E., Harnik, Y., Ben-Moshe, S., Massasa, E.E., Rozenberg, M., Eilam, R., et al., 2018. Spatial reconstruction of single enterocytes uncovers broad zonation along the intestinal villus Axis. Cell 175(4):1156—1167 e1115.

[64] Lieberthal, W., Tang, M., Zhang, L., Viollet, B., Patel, V., Levine, J.S., 2013. Susceptibility to ATP depletion of primary proximal tubular cell cultures derived from mice lacking either the alpha1 or the alpha2 isoform of the catalytic domain of AMPK. BMC Nephrology 14:251.

[65] Ghosh, P., 2017. The stress polarity pathway: AMPK 'GIV'-es protection against metabolic insults. Aging 9(2):303—314.

[66] Aznar, N., Patel, A., Rohena, C.C., Dunkel, Y., Joosen, L.P., Taupin, V., et al., 2016. AMP-activated protein kinase fortifies epithelial tight junctions during energetic stress via its effector GIV/Girdin. Elife 5.

[67] Johnson, A.M., Costanzo, A., Gareau, M.G., Armando, A.M., Quehenberger, O., Jameson, J.M., et al., 2015. High fat diet causes depletion of intestinal eosinophils associated with intestinal permeability. PloS One 10(4):e0122195.

[68] Damms-Machado, A., Louis, S., Schnitzer, A., Volynets, V., Rings, A., Basrai, M., et al., 2017. Gut permeability is related to body weight, fatty liver disease, and insulin resistance in obese individuals undergoing weight reduction. American Journal of Clinical Nutrition 105(1):127—135.

[69] Foretz, M., Guigas, B., Viollet, B., 2019. Understanding the glucoregulatory mechanisms of metformin in type 2 diabetes mellitus. Nature Reviews Endocrinology 15(10):569—589.

[70] Duca, F.A., Cote, C.D., Rasmussen, B.A., Zadeh-Tahmasebi, M., Rutter, G.A., Filippi, B.M., et al., 2015. Metformin activates a duodenal Ampk-dependent pathway to lower hepatic glucose production in rats. Nature Medicine 21(5):506—511.

[71] Everard, A., Belzer, C., Geurts, L., Ouwerkerk, J.P., Druart, C., Bindels, L.B., et al., 2013. Cross-talk between Akkermansia muciniphila and intestinal epithelium controls diet-induced obesity. Proceedings of the National Academy of Sciences of the USA 110(22):9066—9071.

[72] Harmel, E., Grenier, E., Bendjoudi Ouadda, A., El Chebly, M., Ziv, E., Beaulieu, J.F., et al., 2014. AMPK in the small intestine in normal and pathophysiological conditions. Endocrinology 155(3):873—888.

[73] Wu, W., Wang, S., Liu, Q., Shan, T., Wang, X., Feng, J., et al., 2020. AMPK facilitates intestinal long-chain fatty acid uptake by manipulating CD36 expression and translocation. The FASEB Journal 34(4):4852—4869.

[74] Turner, J.R., 2009. Intestinal mucosal barrier function in health and disease. Nature Reviews. Immunology 9(11):799—809.

[75] Sun, X., Du, M., Navarre, D.A., Zhu, M.J., 2018. Purple potato extract promotes intestinal epithelial differentiation and barrier function by activating AMP-activated protein kinase. Molecular Nutrition & Food Research 62(4).

[76] Park, H.Y., Kunitake, Y., Hirasaki, N., Tanaka, M., Matsui, T., 2015. Theaflavins enhance intestinal barrier of Caco-2 Cell monolayers through the expression of AMP-activated protein kinase-mediated Occludin, Claudin-1, and ZO-1. Bioscience Biotechnology & Biochemistry 79(1):130—137.

[77] Xiang, R.L., Mei, M., Cong, X., Li, J., Zhang, Y., Ding, C., et al., 2014. Claudin-4 is required for AMPK-modulated paracellular permeability in submandibular gland cells. Journal of Molecular Cell Biology 6(6):486—497.

[78] Zhang, L., Jouret, F., Rinehart, J., Sfakianos, J., Mellman, I., Lifton, R.P., et al., 2011. AMP-activated protein kinase (AMPK) activation and glycogen synthase kinase-3β (GSK-3β) inhibition induce Ca2+-independent deposition of tight junction components at the plasma membrane. Journal of Biological Chemistry 286(19):16879—16890.

[79] Evers, S.S., Sandoval, D.A., Seeley, R.J., 2017. The physiology and molecular underpinnings of the effects of bariatric surgery on obesity and diabetes. Annual Review of Physiology 79:313—334.

[80] Amouyal, C., Castel, J., Guay, C., Lacombe, A., Denom, J., Migrenne-Li, S., et al., 2020. A surrogate of Roux-en-Y gastric bypass (the enterogastro anastomosis surgery) regulates multiple beta-cell pathways during resolution of diabetes in ob/ob mice. EBioMedicine 58:102895.

[81] Sayers, S.R., Reimann, F., Gribble, F.M., Parker, H., Zac-Varghese, S., Bloom, S.R., et al., 2016. Proglucagon promoter Cre-mediated AMPK deletion in mice increases circulating GLP-1 levels and oral glucose tolerance. PloS One 11(3):e0149549.

[82] Dusaulcy, R., Handgraaf, S., Skarupelova, S., Visentin, F., Vesin, C., Heddad-Masson, M., et al., 2016. Functional and molecular adaptations of enteroendocrine L-cells in male obese mice are associated with preservation of pancreatic α-cell function and prevention of hyperglycemia. Endocrinology 157(10):3832—3843.

[83] Waise, T.M.Z., Rasti, M., Duca, F.A., Zhang, S.Y., Bauer, P.V., Rhodes, C.J., et al., 2019. Inhibition of upper small intestinal mTOR lowers plasma glucose levels by inhibiting glucose production. Nature Communications 10(1):714.

[84] Koh, A., Mannerås-Holm, L., Yunn, N.O., Nilsson, P.M., Ryu, S.H., Molinaro, A., et al., 2020. Microbial imidazole propionate affects responses to metformin through p38γ-dependent inhibitory AMPK phosphorylation. Cell Metabolism.

[85] Li, Q., Zhang, M., Wu, T., Liu, R., 2020. Potential correlation between carbohydrate-active enzyme family 48 expressed by gut microbiota and the expression of intestinal epithelial AMP-activated protein kinase β. Journal of Food Biochemistry 44(2):e13123.

[86] Håkansson, Å., Tormo-Badia, N., Baridi, A., Xu, J., Molin, G., Hagslätt, M.L., et al., 2015. Immunological alteration and changes of gut microbiota after dextran sulfate sodium (DSS) administration in mice. Clinical and Experimental Medicine 15(1):107—120.

[87] Rowan, F., Docherty, N.G., Murphy, M., Murphy, B., Calvin Coffey, J., O'Connell, P.R., 2010. Desulfovibrio bacterial species are increased in ulcerative colitis. Diseases of the Colon & Rectum 53(11):1530—1536.

 